Contact inhibitory Eph signaling suppresses EGF-promoted cell migration by decoupling EGFR activity from vesicular recycling

Wayne Stallaert[1], Ola Sabet[1], Yannick Brüggemann[1,2], Lisa Baak[1] and Philippe I.H. Bastiaens[1,2*]

Affiliations

[1]Department of Systemic Cell Biology, Max Planck Institute of Molecular Physiology, Otto-Hahn-Str.11, 44227 Dortmund, Germany

[2]Faculty of Chemistry and Chemical Biology, TU Dortmund, Otto-Hahn-Str. 6, 44227 Dortmund, Germany

*Correspondence to: philippe.bastiaens@mpi-dortmund.mpg.de

Summary:

Eph receptor activation generates context-dependent cellular responses to EGFR activation by altering its vesicular trafficking dynamics.

Abstract

The ability of cells to adapt their behavior to growth factors in relation to their environment is an essential aspect of tissue development and homeostasis. Here we show that Eph receptor signaling from cell-cell contacts changes the cellular response to EGFR activation by altering its vesicular trafficking. Eph receptor activation traps EGFR in Rab5-positive early endosomes through an inhibition of Akt-dependent vesicular recycling. By altering the spatial distribution of EGFR activity during EGF stimulation, Eph receptor activation selectively suppresses migratory Akt signaling from the plasma membrane, while preserving proliferative ERK signaling from endosomes. We also show that soluble extracellular signals engaging the G-protein coupled receptor Kiss1 similarly suppress vesicular recycling to alter EGFR signaling. The cellular environment can thus modulate EGFR vesicular trafficking dynamics to generate context-dependent responses to EGF stimulation.

Introduction

Activation of epidermal growth factor receptor (EGFR) promotes a variety of cellular responses including cell growth, proliferation, survival, apoptosis, differentiation and migration (*1*), some of which are functionally opposed. To select among these diverse outcomes, the cell requires additional contextual information. This context can be intrinsic (e.g. cell type or cell cycle stage), or extrinsic, in the form of extracellular signals that provide information about the current (or past) environmental context. Adaptability to a changing environment requires that extrinsic information be integrated through mechanisms that can transform the response to subsequent growth factor stimulation.

Local cell density is one such example of extrinsic context that can influence cellular activity to generate distinct functional states (*2-4*). The Eph family of receptor tyrosine kinases act as sensors of cell density, becoming activated at points of cell-cell contact through interactions with membrane bound ephrin ligands presented on the surfaces of adjacent cells (*5*). Eph receptors in many ways operate in functional opposition to EGFR, acting as tumour suppressors (*5-11*) and mediating contact inhibition of locomotion to suppress cellular migration and metastasis (*12-15*). Moreover, a functional coupling of EGFR and Eph receptor activity has been shown to control cell migration (*15*). Although the precise mechanism through which Eph receptors regulate EGF-promoted migration remains elusive, a convergence of receptor activity on phosphoinositide 3-kinase (PI3K)/Akt signaling was implicated.

Akt has been shown to regulate EGFR vesicular trafficking through the endosomal system (*16*). By stimulating the activity of the early endosomal effector PIKfyve (FYVE-

containing phosphatidylinositol 3-phosphate 5-kinase), Akt activity controls the transition of EGFR through early endosomes, regulating both its recycling back to the PM and its degradation in the lysosome. Thus, while endocytosis of cell surface receptors has traditionally been viewed as a mechanism to attenuate downstream signaling following ligand stimulation, the notion that signaling molecules downstream of cell surface receptors can, in turn, influence vesicular trafficking (*16-21*) generates a reciprocal relationship between receptor activation and vesicular dynamics whose role in shaping the cellular response to stimuli has only recently begun to garner attention (*22*). Furthermore, this bidirectional relationship could also allow the signaling activity of one receptor to influence the response properties of another through changes in its vesicular trafficking dynamics, generating context-dependent receptor activity.

In the current work, we show that Eph receptor activation at cell-cell contacts regulates the vesicular dynamics of EGFR through an inhibition of Akt-dependent trafficking. By modulating the spatial distribution of EGFR activity, Eph receptor activation alters the cellular response to EGF stimulation, selectively suppressing EGF-promoted migratory signaling while preserving its effect on proliferation.

RESULTS

Eph receptor activation affects EGFR vesicular trafficking

Stimulation of endogenous Eph receptors in Cos-7 cells with a soluble, clustered ephrinA1-Fc (A1) ligand (*23, 24*) induced a reduction in EGFR abundance at the PM (**Fig. 1A-B**). This decrease in PM EGFR abundance following Eph receptor activation was observed in various cell lines, including HEK293, NIH 3T3, MCF10A and MDA-MB-231 cells (**Fig. S1A-D**), exhibiting a wide range of endogenous EGFR expression (**Fig. S1E**).

While EGFR internalization is a well-established consequence of growth factor-induced receptor activation, we observed that the loss of PM EGFR did not result from an Eph receptor-induced transactivation of EGFR (**Fig S1F**). Since EGFR also continuously recycles through the endosomal system in the absence of growth factor stimulation (*25*), we hypothesized that Eph receptor activation may reduce PM EGFR abundance by trapping constitutively recycling receptors in endosomes.

Eph receptor activation decreases the activity of Akt (**Fig. 1C**)(*14*) , a signaling effector previously demonstrated to promote EGFR vesicular recycling (*16*). Direct inhibition of Akt or its downstream early endosomal effector PIKfyve (*16*) indeed reduced PM EGFR abundance in Cos-7 cells (**Fig. 1D-E**). A1 stimulation or PIKfyve inhibition promoted similar decreases in PM EGFR abundance, as measured by a reduction in PM EGF-Alexa647 binding (**Fig. 1E**). Furthermore, the combination of Eph receptor activation with PIKfyve inhibition did not further reduce PM EGFR abundance (**Fig. 1E**), indicative of a shared molecular mechanism. Consistent with a suppression of constitutive EGFR recycling, we observed an endosomal accumulation of ectopically expressed EGFR-mCherry in live cells after Akt or PIKfyve inhibition (**Fig. 1F, Movie S1, Fig. S2A-B**). Time lapse confocal imaging of Cos-7 cells expressing EGFR-mCherry and EphA2-mCitrine also revealed an endosomal accumulation of EGFR with time following soluble A1 stimulation (**Fig. 1G-I, Movie S2**) or upon presentation of ephrinA1 ligand on the membrane of adjacent cells at sites of cell-cell contact (**Movie S3**). This shift in the spatial distribution of EGFR from the PM to endosomes following A1 stimulation occurred primarily by trapping receptors in Rab5-positive early endosomes (**Fig. 1J**), consistent with an inhibition of Akt-dependent trafficking (*16*) (**Fig. 1J**). Thus, Eph receptor activation alters the subcellular distribution of EGFR prior to growth factor

stimulation by trapping constitutively recycling receptors in Rab5-positive early endosomes through an inhibition of Akt/PIKfyve-dependent vesicular recycling.

We next investigated how Eph receptor activation influences EGFR trafficking during EGF stimulation. The trafficking fate of EGFR through the endosomal system is determined by post-translational modifications, with receptor ubiquitination acting as a molecular switch that diverts EGFR to the lysosome for degradation (*25*). Since EGFR ubiquitination increases with EGF binding (*26*), saturating EGF concentrations (> 50 ng/ml (*27*)) generate a finite temporal signaling response by progressively depleting PM EGFR through ubiquitin-dependent lysosomal degradation. Stimulation of endogenous receptors in Cos-7 cells with a saturating concentration of EGF (100 ng/ml) induced a ~40% reduction in total EGFR expression after 60 min of stimulation (**Fig. S2C**) and residual EGFR resided primarily in Rab7-positive late endosomes (**Fig. 1J**). A1 pretreatment or direct Akt inhibition, in contrast, impaired Rab5-to-Rab7 endosomal maturation (*28*) (**Fig. 1J**), leading to a reduction in receptor degradation at saturating EGF concentrations (≥50 ng/ml; **Fig. S2C**).

At lower, subsaturating EGF concentrations typically found in human tissue secretions (0.4-20 ng/ml)(*29*), only a fraction of receptors are ligand bound, receptor ubiquitination is reduced (*26*), and internalized receptors are preferentially recycled back to the PM (*30*). To assess whether Eph receptors inhibit EGFR recycling following subsaturating EGF stimulation, we pulsed endogenous receptors in Cos-7 cells with 10 ng/ml EGF to induce EGFR endocytosis and measured its subsequent return to the PM following EGF washout (**Fig. 1K**). While we observed a complete recovery of PM EGFR

abundance in control cells following EGF washout, A1 pretreatment completely suppressed EGFR recycling.

Thus, Eph receptor activation suppresses EGFR trafficking through the early endosome during EGF stimulation; impairing the recycling of non-ubiquitinated receptors back to the PM as well as inhibiting the transition of ubiquitinated receptors to late endosomes.

Eph receptor activation changes the spatial distribution of EGFR activity

Many functional outcomes to EGFR activation, such as cellular migration, require that cells remain responsive to persistent growth factor stimulation. To ensure sensitivity to stimuli during long periods of exposure, the cell must maintain sufficient receptor abundance at the PM despite the continuous internalization of activated receptors. We therefore posed the following questions: Does Akt-dependent recycling help maintain cellular responsiveness to EGF during persistent, subsaturating stimulation? Can Eph receptor activation at cell-cell contacts change the response properties of EGFR by modulating its vesicular trafficking?

To address the impact of Akt-dependent recycling on EGFR activation, measurements of endogenous EGFR phosphorylation and trafficking in Cos-7 cells were obtained by immunofluorescence following subsaturating EGF stimulation in control cells and following Eph receptor activation or Akt/PIKfyve inhibition. Individual cells were radially segmented to quantify changes in the average spatial distribution of EGFR activity with time and visualized using 3-D spatial-temporal maps (**Fig. 2A**). Through an accumulation of EGFR in endosomal compartments during sustained EGF stimulation, cells pretreated with either A1 or an Akt inhibitor generated less EGFR phosphorylation

after 60 min of EGF stimulation relative to control cells (**Fig. 2A-B**). Decoupling Akt activation from its effect on trafficking by PIKfyve inhibition had indistinguishable effects from direct Akt inhibition or A1 pretreatment on EGFR phosphorylation and trafficking (**Fig. 2A-B**), indicating that Akt activity maintains EGFR activation at the PM during sustained, subsaturating EGF stimulation through its effects on vesicular recycling.

To specifically quantify EGFR phosphorylation at the PM and on endosomes during sustained, subsaturating EGF stimulation, we employed fluorescence lifetime imaging microscopy (FLIM) to detect Förster resonance energy transfer (FRET) between EGFR-mCitrine and a phospho-tyrosine binding domain fused to mCherry (PTB-mCherry) (*31*) in Cos-7 cells (**Fig. 2C-F**). In control cells, EGFR-mCitrine remained highly phosphorylated at both the PM and in endosomes following 60 min of sustained EGF-Alexa647 stimulation. In cells pretreated with A1 or following Akt or PIKfyve inhibition, we observed reduced PM EGFR-mCitrine density (**Fig. 2D**) and EGF-Alexa647 binding (**Fig. 2E**), resulting in diminished EGFR-mCitrine phosphorylation specifically at the PM (**Fig. 2F**). In these conditions in which Akt-dependent recycling was suppressed, ligand-bound, active EGFR-mCitrine accumulated in endosomes, maintaining its phosphorylation in this compartment to the same extent as control cells (**Fig. 2C-F**).

Eph receptor activation, therefore, by inhibiting Akt-dependent recycling, changes the spatial distribution of EGFR activity during sustained, subsaturating EGF stimulation, selectively reducing EGFR activation at the PM while preserving receptor activity in endosomes.

184 ***Eph receptor activation at cell-cell contact alters the EGFR signaling response***

185 Although EGFR continues to activate signaling effectors from endosomal membranes
186 (*32-40*), Akt is preferentially activated at the PM (*41, 42*) (**Fig. S3**). We therefore
187 investigated how Eph receptor activation, by changing the spatial distribution of EGFR
188 activity, regulates its signaling response during EGF stimulation. By suppressing
189 vesicular recycling and reducing EGFR activity at the PM, A1 pretreatment selectively
190 inhibited Akt activation following subsaturating EGF stimulation of endogenous
191 receptors in Cos-7 (**Fig. 3A top, Fig. S4A**) and HEK293 cells (**Fig. S4B**), while ERK
192 activation, which can continue from endosomal membranes (*37, 39, 43*) (**Fig. S3**),
193 remained intact (**Fig 3A bottom, Fig. S4**). To confirm that EphA2 inhibits EGF-promoted
194 Akt activation by suppressing EGFR recycling and does not simply reflect the opposed
195 regulation of Akt by EGFR and EphA2 (activation vs inhibition, respectively), we
196 assessed whether EGFR trafficking was dispensable for the A1-induced suppression of
197 EGF-promoted Akt activation. Cells were prestimulated with A1, followed by treatment
198 with the dynamin inhibitor dynole 34-2 to block subsequent endocytosis, and then
199 stimulated with EGF. When EGFR endocytosis was blocked (**Fig. S3C**), A1 pretreatment
200 had no effect on EGF-promoted Akt activation (**Fig. 3B top**). Pretreatment with the
201 negative control analogue dynole 31-2, to control for off-target effects, did not inhibit
202 EGFR endocytosis (**Fig. S3C**), and had no effect on A1-induced suppression of EGF-
203 promoted Akt activation (**Fig. 3B bottom**), corroborating that intact EGFR vesicular
204 trafficking is required for the inhibitory effect of Eph receptors on EGFR signaling.
205
206 Increasing concentrations of A1 progressively inhibited EGF-mediated Akt activation
207 (**Fig. 3C**), suggesting that the degree of cell-cell contact might determine the magnitude
208 of Akt activation in response to a given concentration of EGF. To directly investigate the

209 influence of cell-cell contact on EGFR signaling, we obtained single cell measurements of
210 Akt and ERK activation in Cos-7 with varying degrees of cell-cell contact. Homotypic cell-
211 cell contact promotes Eph receptor activation through interactions with ephrins
212 presented on neighboring cells (*24*) (**Fig. 3D**). Akt activation decreased with cell-cell
213 contact both prior to and following EGF stimulation (**Fig. 3E**), demonstrating that
214 increasing cell-cell contact reduces the magnitude of EGF-promoted Akt activation. ERK
215 activation, on the other hand, was unaffected by cell-cell contact, with cells generating
216 similar EGF-promoted increases in ERK activation irrespective of their degree of cell-cell
217 contact (**Fig. 3F**).
218
219 ***Coupling EGFR activity to vesicular recycling generates a positive feedback***
220 While the inhibition of Akt-dependent recycling results in a reduction in PM EGFR
221 abundance in Cos-7 cells (**Fig. 1A-K, Fig. S1A-D, Fig. S2A-B**), we also observed that an
222 increase in cellular Akt activity through the inhibition of its negative regulator PP2A by
223 okadaic acid resulted in a concomitant increase in PM EGFR (**Fig. 4A**). Since EGFR
224 activation itself increases Akt activity in cells (**Fig. 3A-C, Fig. 3E, Fig. S3**), we next asked
225 whether PM EGFR abundance is actively maintained during growth factor stimulation
226 through an EGF-induced increase in Akt-dependent vesicular recycling. Using a
227 fluorescence localization after photoactivation (FLAP) approach to quantify the
228 vesicular trafficking of EGFR to the PM following photoactivation of EGFR-paGFP in
229 endosomes (**Fig. 4B top**), we observed an increase in EGFR-paGFP recycling during EGF
230 stimulation (**Fig. 4B bottom**). Akt inhibition completely suppressed this EGF-promoted
231 increase in vesicular recycling (**Fig. 4B bottom**), further demonstrating the contribution
232 of Akt-dependent recycling in sustaining PM EGFR activity (**Fig. 3A**). Thus, by

stimulating Akt-dependent recycling, EGFR activation generates a positive feedback that actively maintain its PM abundance during EGF stimulation.

Positive feedback in combination with inhibitory network motifs can convert graded inputs into switch-like, ultrasensitive signaling responses (*44*). Since Akt is preferentially activated at the PM (**Fig. S4**), the EGF-induced increase in EGFR vesicular recycling (**Fig. 4B**) could generate a positive feedback for Akt activation (**Fig. 4C**). To investigate if this positive feedback can generate a switch-like activation of Akt, we measured Akt phosphorylation in thousands of individual Cos-7 cells by flow cytometry following sustained stimulation with a range of EGF concentrations (**Fig. 4D-E**). Cells were stimulated in suspension to negate in situ cell-cell contact as an extrinsic source of variability in Akt activation (**Fig. 3E**). At concentrations ≥ 1 ng/ml, EGF stimulation produced a switch-like activation to a high Akt phosphorylation state in a subpopulation of cells, whose proportion increased with EGF concentration (**Fig. 4D-E top**). Decoupling EGFR activation from its effect on vesicular recycling by PIKfyve inhibition (**Fig. 4D-E middle**) or A1 pretreatment (**Fig. 4D-E bottom**) did not result in a global decrease in cellular Akt activation but rather reduced the proportion of cells generating a high Akt phosphorylation state, consistent with the inhibition of a positive feedback that produces this switch-like response. Intrinsic cell-to-cell variability in the EGF threshold required to stimulate Akt-dependent vesicular recycling, therefore, determines the proportion of cells that transition to a high Akt activity state at a given EGF concentration. Eph receptor activation, by decoupling EGFR activation from its effect on vesicular trafficking, reduces Akt activation within the population by decreasing the proportion of cells transitioning to a high Akt activity state during EGF stimulation.

Eph activation at cell-cell contact suppresses the EGF-promoted transition to a migratory state

EGFR signaling to effectors at the PM generates exploratory cellular behaviors (*45-52*) that must be maintained to induce a persistent migratory response. Given that contact inhibitory Eph receptor activation selectively suppresses PM signaling during sustained, subsaturating EGF stimulation (**Fig. 3A, 4D-E**), we investigated if cell-cell contact regulates EGF-promoted migration by inhibiting Akt-dependent recycling. Since Cos-7 cells exhibit limited migratory behavior, we examined NIH 3T3 mouse embryonic fibroblast (MEF) cells, which generate a haptotactic migratory response to fibronectin that is enhanced by EGF through an increase in exploratory behavior (*53*). Similar to Cos-7 cells (**Fig. 1A-B**), these cells also exhibit a Eph-activity dependent depletion of PM EGFR abundance (**Fig. 5A-B**). Following stimulation with a subsaturating EGF concentration (20 ng/ml), we observed a significant increase in the proportion of migratory cells (**Fig. 5C top, Movie S4, Fig. S5**), but no change in the average distance travelled per cell (**Fig. 5C bottom**). This indicates that EGF promotes the transition of individual cells to a migratory state rather than increasing overall cellular motility. Since EGF binding promotes receptor ubiquitination and degradation, sustained stimulation with supraphysiological saturating EGF concentrations (100 ng/ml) induces a rapid loss in EGF sensitivity with time and thus did not significantly increase the proportion of migratory cells (**Fig. 5C top**). Decoupling EGFR activation from its effect on Akt-dependent recycling through the inhibition of PIKfyve or following Eph receptor activation decreased the proportion of migratory cells (**Fig. 5C top**). We observed further that increasing concentrations of A1 progressively decreased EGF-induced migration (**Fig. 5C top**), consistent with its concentration-dependent effect on EGF-

promoted Akt activation (**Fig. 3C**) and suggesting that the amount of ephrinA1-Eph receptor interactions at points of cell-cell contact may determine whether a cell initiates a migratory response to EGF. Indeed, we found that the number of migratory cells following EGF stimulation was inversely proportional to cell density (**Fig. 5D**) and that the increase in migration observed at low densities could be countered by treatment with soluble A1 to mimic Eph receptor contact inhibitory signaling (**Fig. 5D**). Thus, physiological Eph receptor activation at points of homotypic cell-cell contact suppresses EGF-promoted migration by inhibiting Akt-dependent vesicular recycling. However, by preserving endosomal ERK activation following EGF stimulation (**Fig. 3A bottom**), we found that neither PIKfyve inhibition nor A1 pretreatment led to a reduction in EGF-promoted cell proliferation (**Fig. 5E**). Thus, by altering the spatiotemporal distribution of EGFR activity, contact inhibitory signaling by Eph receptors influences the cellular outcome to EGF stimulation, preserving a proliferative response while suppressing cell migration.

Modulation of vesicular dynamics as a general mechanism to produce context-dependent EGFR signaling

To determine whether environmental signals other than cell-cell contact can influence EGFR signaling through changes in its vesicular trafficking, we investigated the effect of activation of the G protein-coupled receptor Kiss1 (Kiss1R), which, similar to Eph receptors, inhibits Akt (*54*) and suppresses cell migration and metastatic invasion (*55*). Stimulation with the soluble Kiss1R ligand kisspeptin-10 (Kp-10) reduced Akt activity in HEK293 cells and decreased PM EGFR abundance (**Fig. 6A**). Similar to the effect of cell-cell contact, pretreatment with Kp-10 selectively inhibited EGF-promoted Akt activation

(**Fig. 6B**), while preserving ERK activation (**Fig. 6C**). The modulation of EGFR vesicular trafficking dynamics could therefore provide a general mechanism to generate plasticity in the signaling response to EGFR activation, through which diverse environmental signals such as cell-cell contact or soluble stimuli like Kp-10 can influence the cellular response to EGF.

DISCUSSION

In this paper, we demonstrate that Eph receptor activation at cell-cell contacts can generate context-dependent cellular responses to EGF stimulation by modulating EGFR vesicular trafficking dynamics.

Chemotaxis requires that cells remain responsive to stimuli for prolonged periods of time as they migrate toward the chemotactic source. Through an increase in Akt-dependent recycling (**Fig. 4B**), EGF stimulation maintains EGFR density at the PM during persistent, subsaturating stimulation. Since Akt itself is preferentially activated at the PM (**Fig. S3**), the EGF-promoted increase in vesicular recycling generates a positive feedback that switches cells to a high Akt activation state (**Fig. 4D-E**). Although Akt has been previously observed on endosomal membranes through interactions with the early endocytic adaptor protein APPL1 (*56, 57*), de novo activation of Akt by EGFR requires the production of $PI(3,4,5)P_3$, which is impeded by the low abundance of $PI(4,5)P_2$ in endosomal membranes (*41, 58*). Although Akt activation may occur to some extent on endosomal membranes (*59*), since the coupling of active EGFR to Akt activation will be more efficient at the PM, any perturbations that influence the spatial distribution of

EGFR, such as Eph receptor activation, will influence the capacity of EGFR to activate Akt (**Fig. 3A, Fig. 6A-B, Fig. S3**).

We observed that the switch to a high Akt activity state only occurs in a proportion of cells, even in the absence of in situ cell-cell contacts, and increases with EGF concentration (**Fig. 4D-E**). Population heterogeneity in Akt activation has been previously attributed to cell-to-cell variation in PI3K expression (*60*). Our data suggest that intrinsic variability in the expression of signaling and/or trafficking effectors may determine, for a given cell, the EGF concentration required to stimulate Akt-dependent trafficking and engage the positive feedback that produces a high Akt activity state. Small differences in EGF concentration substantially influence the proportion of cells generating a high Akt response (e.g. a shift from 5 to 10 ng/ml increases the proportion of cells from 43 to 85%, respectively, **Fig. 4D-E**). Perhaps it is not coincidental that the concentration range over which this switch occurs corresponds to the physiological range of EGF concentrations (*29*). By generating a sharp boundary for Akt activation within the physiological EGF concentration regime, even slight changes in the threshold of this switch could have profound implications for tissue dynamics (e.g. initiation of migration).

Eph receptor activation, for example, by suppressing EGFR recycling, decreased the proportion of cells generating a high Akt response from 85 to 41% in response to 10 ng/ml EGF (**Fig. 4D-E**). The dependence of Akt activation on EGFR recycling allows the degree of cell-cell contact to regulate the proportion of cells generating a migratory response to EGF stimulation. PI3K/Akt signaling has previously been suggested as the point of convergence for EGFR/Eph control of cell migration (*15*); however, the

358 molecular mechanism underlying this oppositional relationship remained unclear. Our
359 results indicate that Eph receptor activation inhibits EGF-promoted cell migration by
360 suppressing Akt-dependent recycling, thus impeding the spatially-maintained positive
361 feedback that generates a high Akt response and decreasing the sensitivity of cells to
362 persistent EGF stimulation necessary to maintain exploratory behavior. However, by
363 changing the spatial distribution of EGFR activity (**Fig. 2C-D**), Eph receptor activation
364 selectively suppresses migratory signaling from the PM while leaving proliferative ERK
365 signaling intact (**Fig. 3A, Fig. 3E-F, Fig. 5C-D**). This contextual plasticity generates two
366 distinct cellular outcomes to EGF stimulation that may be important in physiological
367 settings such as wound healing. At the tissue boundary, cells with reduced cell-cell
368 contact would increase their exploratory behavior in response to EGF released at the
369 site of the wound. Cells located deeper in the tissue, despite extensive cell-cell contact,
370 would retain their proliferative response to extracellular EGF, and undergo mitosis to fill
371 the vacant space created as exploratory cells migrate to occupy the wound area.
372
373 Our observations demonstrate that communication between receptors with opposed
374 functionality can emerge through changes in vesicular trafficking dynamics rather than
375 relying on direct interactions between the receptors or their respective effectors. Such a
376 mechanism also allows different receptors with similar functional roles (e.g. EphA2 and
377 Kiss1R) to alter the cellular response to stimuli without having to evolve distinct protein
378 interaction domains to do so. The dependency of EGFR signaling on its vesicular
379 dynamics could confer a general mechanism through which the cell can generate
380 functional plasticity to growth factor stimulation while preserving specificity in cell-cell
381 communication.
382

383

384

385

386

Materials and methods

Primary antibodies

Mouse anti-Akt (2920, Cell Signaling Technology (CST), Danvers, MA, USA), mouse anti-Akt-Alexa488 (2917, CST), rabbit anti-phospho-Akt(Ser^{473}) (4060, CST), rabbit anti-phospho-Akt (Ser^{473})-Alexa647 (4075, CST), mouse anti-HA (9658, Sigma-Aldrich, St.Louis, MO, USA), rabbit anti-EGFR (4267, CST), goat anti-EGFR (AF231, R&D Systems, Minneapolis, MN, USA), mouse anti-phospho-EGFR(Tyr^{845}) (558381, BD Biosciences, Heidelberg, Germany), rabbit anti-phospho-EGFR(Tyr^{1045}) (2237, CST), mouse anti-phospho-EGFR(Tyr^{1068}) (2236, CST), goat anti-EphA2 (R&D Systems), rabbit anti-phospho-Eph(Tyr$^{588/596}$) (Abcam, Cambridge, UK), mouse anti-ERK1/2 (4696, CST), rabbit anti-phospho-ERK(Thr$^{202/Tyr204}$) (4370, CST), mouse anti-Rab5 (610724, BD Biosciences), rabbit anti-Rab7 (9367, CST), rabbit anti-phospho-Rb(Ser807/811, CST) mouse anti-tubulin (6074, Sigma-Aldrich)

Secondary antibodies

IRDye 680RD Donkey anti-Mouse (LI-COR Biosciences), IRDye 680RD Donkey anti-Rabbit (LI-COR Biosciences), IRDye 680RD Donkey anti-Goat (LI-COR Biosciences), IRDye 800CW, Donkey anti-Mouse (LI-COR Biosciences), IRDye 800CW Donkey anti-Rabbit (LI-COR Biosciences), IRDye 800CW Donkey anti-Rabbit (LI-COR Biosciences), AlexaFluor 405 goat anti-Mouse (Life Technologies), AlexaFluor 488 donkey anti-Goat (Life Technologies), AlexaFluor 546 donkey anti-rabbit (Life Technologies), AlexaFluor 647 donkey anti-Rabbit (Life Technologies)

Plasmids

412 Generation of EGFR-mCitrine, EGFR-mCherry, EGFR-paGFP, PTB-mCherry, c-Cbl-BFP
413 and HA-ubiquitin (*25*), as well as EphA2-mCitrine, SH2-mCherry and LIFEA2 (*24*) were
414 previously described. pcDNA3.1-EphA2 was a gift from Tony Pawson.
415
416 *Reagents*
417 AktVIII (sc-3513, Santa Cruz Biotechnology, Dallas, TX, USA), EGF (AF-100-15,
418 Peprotech, Hamburg, Germany), okadaic acid (sc-3513, Santa Cruz Biotechnology),
419 YM201636 (13576, Biomol GmbH, Hamburg, Germany), dynole 31-2 (ab120464,
420 Abcam), dynole 34-2 (ab120463, Abcam), Kisspeptin-10 (445888, Merck Millipore).
421 EGF-Alexa647 was prepared as previously described (*25*). EphrinA1-Fc (602-A1-200)
422 was preclustered by incubating with chicken Anti-Fc (GW200083F, Sigma-Aldrich) at a
423 ratio of 5:1 at room temperature for at least 30 min.
424
425 *Cell culture*
426 Cos-7, HEK293 and NIH 3T3 cells were grown in Dulbecco's Modified Eagle's Medium
427 (DMEM) supplemented with 10% fetal bovine serum (FBS), 2 mM L-glutamine and 1%
428 non-essential amino acids (NEAA) and maintained at 37°C in 5% CO_2. MCF10A cells
429 were grown in DMEM/F12 supplemented with 5% horse serum, 20 ng/ml EGF, 500
430 ng/ml hydrocortisone, 100 ng/ml cholera toxin and 10 µg/ml insulin and maintained at
431 37°C in 5% CO_2. MDA-MB-231 cells were grown in Leibowitz medium supplemented
432 with 10% FBS and 2mM L-glutamine maintained at 37°C in 0% CO_2. When required,
433 transfection of cells was performed using FUGENE6 (Roche Diagnostics, Mannheim,
434 Germany) or Lipofectamine 2000 (Life Technologies, Darmstadt, Germany) according to
435 manufacturer's protocol. Approximately 16-18 hours prior to an experiment, cells were
436 starved in DMEM containing 0.5% FBS, 2 mM L-glutamine and 1% NEAA. One hour

437 before stimulation, starvation media was changed to serum-free DMEM or DMEM
438 without phenol red for live cell imaging. Unless explicitly stated in the figure legends, all
439 experiments were performed with Cos-7 cells with endogenous expression of EGFR and
440 Eph receptors.
441
442 *In-cell westerns (ICW) and on-cell westerns (OCW)*
443 Cells were seeded on black, transparent bottomed 96-well plates (3340, Corning, Hagen,
444 Germany) coated with poly-L-lysine (P6282, Sigma Aldrich). Cell were fixed with Roti-
445 Histofix 4% (Carl Roth, Karsruhe, Germany) for 5 min at 37°C. For ICW, cells were
446 permeabilized with 0.1% Triton X-100 (v/v) for 5 min at room temperature. For OCW,
447 cells were not permeabilized. Samples were incubated in Odyssey TBS blocking buffer
448 (LI-COR Biosciences, Lincoln, NE, USA) for 30 min at room temperature. Primary
449 antibodies were incubated overnight at 4°C and secondary antibodies (IRDyes, LI-COR
450 Biosciences) were incubated in the dark for 1 h at room temperature. All wash steps
451 were performed with TBS (pH 7.4). Intensity measurements were made using the
452 Odyssey Infrared Imaging System (LI-COR Biosciences). ICW/OCW were calibrated by
453 Western blots to ensure accurate quantification. Quantification of the integrated
454 intensity in each well was performed using the MicroArray Profile plugin (OptiNav Inc.,
455 Bellevue, WA, USA) for ImageJ v1.47 (http://rsbweb.nih.gov/ij/). In each ICW or OCW,
456 2-4 replicates per conditions were obtained per experiment, and all data presented
457 represents means ± s.e.m. from at least three independent experiments.
458
459 *Immunofluorescence*
460 Cells were cultured on 4- or 8-well chambered glass slides (Lab-tek, Thermo Fisher
461 Scientific, Waltham, MA) and fixed with 4% paraformaldehyde/PBS (w/v) for 10 min at

4°C. To measure PM EGFR, fixed, non-permeabilized samples were first incubated with primary antibody directed at an extracellular epitope of EGFR (AF231, R&D Systems, 1:200) overnight at 4°C followed by secondary antibody for 1 h at room temperature. For all other immunofluorescence experiments, samples were permeabilized with 0.1% Triton X-100 (v/v) for 5 min at room temperature prior to incubation with primary antibodies. All wash steps were performed with TBS (pH 7.4). Fixed samples were imaged in PBS at 37°C. For all analysis, an initial background subtraction was performed on immunofluorescence images. To quantify the proportion of EGFR in Rab5 and Rab7 compartments, binary masks were generated from intensity thresholded images of Rab5 and Rab7 staining. To generate a mask of Rab5/Rab7 double positive endosomes, the product of their individual masks was used. The integrated fluorescence intensity of EGFR-mCherry was determined in each of the endosomal masks and divided by the total integrated EGFR fluorescence intensity of the cell. All analysis was performed using ImageJ. A cell segmentor tool was developed in-house in Anaconda Python (Python Software Foundation, version 2.7, https://www.python.org/) to quantify the spatial distribution of EGFR and pTyr^{845}-EGFR in fixed cells. Cells were divided into 6 equally spaced radial bins emanating from the center of cell mass.

Confocal imaging

Routinely, cells were cultured for live cell confocal imaging on 4- or 8-well chambered glass slides (Lab-tek) and transiently transfected as described above. Confocal images were recorded using an Olympus Fluoview FV1000 confocal microscope (Olympus Life Science Europa, Hamburg, Germany) or a Leica SP8 confocal microscope (Leica Microsystems, Wetzlar, Germany).

Olympus Fluoview™ FV1000

The Olympus Fluoview™ FV1000 confocal microscope was equipped with a temperature controlled CO_2 incubation chamber at 37°C (EMBL, Heidelberg, Germany) and a 60x/1.35 NA Oil UPLSApo objective (Olympus, Hamburg, Germany). EphA2-mCitrine and EGFR-mCherry were excited using a 488 nm Argon-laser (GLG 3135, Showa Optronics, Tokyo, Japan) and a 561 nm DPSS laser (85-YCA-020-230, Melles Griot, Bensheim, Germany), respectively. Detection of fluorescence emission was restricted with an Acousto-Optical Beam Splitter (AOBS) for mCitrine @ 498-551 nm and mCherry @ 575-675 nm. In all cases, scanning was performed in frame-by-frame sequential mode with 2x frame averaging. The pinhole was set to 250 µm.

Leica SP8

The Leica TCS SP8 confocal microscope was equipped with an environment-controlled chamber (LIFE IMAGING SERVICES, Switzerland) maintained at 37°C and a HC PL APO CS2 1.4 NA oil objective (Leica Microsystems, Wetzlar, Germany). Alexa488-conjugated secondary antibodies, fluorescent fusion proteins containing mCitrine and mCherry, and EGF-Alexa647 were excited using a 470–670 nm white light laser (white light laser Kit WLL2, NKT Photonics, Denmark) at 488, 514 and 561 and 647 nm, respectively. PH-Akt-Cerulean was excited using an Argon Laser at 458 nm. Detection of fluorescence emission was restricted with an AOBS as follows: Cerulean @ 468-505 nm, Alexa488 @ 498-551 nm, mCitrine @ 525-570 nm, mCherry @ 570-650 nm and Alexa647 @ 654-754 nm. The pinhole was set to 250 µm and 12-bit images of 512x512 pixels were acquired in a frame-by-frame sequential mode.

Analysis of time-lapse confocal imaging

All analysis of live cell imaging data required an initial background subtraction for all images obtained.

To quantify the proportion of endosomal EGFR-mCherry or EphA2-mCitrine, binary masks of endosomes were generated from intensity thresholded images. The integrated fluorescence intensity of EGFR-mCherry and EphA2-mCitrine was determined in their corresponding endosomal masks and divided by the total integrated fluorescence intensity of the cell.

Fluorescence localization after photoactivation (FLAP) experiments were carried out at 37°C on a Leica SP8. EGFR-mCherry was co-expressed to identify and select regions of endosomal EGFR for photoactivation. Background intensity of EGFR-paGFP prior to photoactivation was measured and subtracted from post-activation images. Photoactivation of EGFR-paGFP was performed with the 405nm laser at 90% power. Following photoactivation, fluorescence images of EGFR-paGFP were acquired every minute for a total of 15 minutes. PM EGFR-paGFP fluorescence was quantified as the integrated intensity in a 5-pixel ring of the cell periphery and, after subtracting pre-activation background intensity, was calculated as a proportion of total EGFR-paGFP intensity.

Fluorescence lifetime imaging microscopy (FLIM)

EGFR-mCitrine, PTB-mCherry and HA-c-Cbl-BFP were ectopically expressed in Cos-7 cells. Fluorescence lifetime measurements of EGFR-mCitrine were performed at 37°C on a Leica SP8 equipped with a time-correlated single-photon counting module (LSM

Upgrade Kit, Picoquant, Berlin, Germany) using a 63x/1.4 NA oil objective. EGFR-mCitrine was excited using a pulsed WLL at a frequency of 20 MHz and fluorescence emission was restricted with an AOBS to 525-570 nm. Photons were integrated for a total of ~ 2 min per image using the SymPhoTime software V5.13 (Picoquant, Berlin, Germany). Data analysis was performed using custom software in Anaconda Python based on global analysis as described in (*61*).

Fluorescence lifetime measurements of LIFEA2 were performed and analyzed as previously described (*24*).

Flow cytometry

Cells were detached using accutase, centrifuged at 200g for 5 min and resuspended in serum-free DMEM. Cells were fixed with 5% sucrose/Roti-Histofix (w/v) for 15 min at 37°C. Ice-cold methanol was added to 90% (v/v) for 30 min on ice. Cells were rinsed once with 0.5% BSA/TBS (w/v) and incubated with Odyssey TBS blocking buffer (LI-COR Biosciences) for 30 min at room temperature. Anti-phospho-Akt(Ser^{473})-Alexa647 (4075, Cell Signaling Technology) was added directly to blocking buffer and incubated overnight at 4°C. Anti-Akt-Alexa488 (2917, Cell Signaling Technology) was added for 2 h prior to measurement. Samples were analyzed using the LSRII flow cytometer (BD Biosciences). Alexa488 was excited with a 488nm laser and fluorescence emission was collected using a 505 nm LP dichroic and a 530/30 nm filter. Alexa647 was excited with 633 nm lasers and fluorescence emission was collected using a 670/40 nm filter. Samples were analyzed using FlowJo v10 (FlowJo, LLC, Ashland, OR, USA) to obtain single cell intensity measurements of phospho- and total Akt. Population distributions of

log(phospho/total Akt) were fitted with a single Gaussian or a sum of two Gaussian distributions using GraphPad Prism (GraphPad Software, La Jolla, CA, USA).

Cell migration

NIH 3T3 cells were seeded onto fibronectin-coated (F0895, Sigma, 1.25 ug/cm^2) 12 well culture dishes (83.3921, Sarstedt, Nuembrecht, Germany) containing 2-well Culture-Inserts (80209, ibidi) to create a cell-free area. Immediately before stimulation, inserts were removed and cells were incubated with Hoechst to label nuclei. Wide field images were acquired using an Olympus IX81 inverted microscope (Olympus, Hamburg, Germany) equipped with a MT20 illumination system, a 4x/0.16 NA air objective and an Orca CCD camera (Hamamatsu Photonics, Hamamatsu City, Japan). Transmission and fluorescence images were acquired every 10 min for 16 h. The cell-free area created by the Culture-Insert was cropped using ImageJ and defined as the migration region. Individual cells were detected and tracked by their nuclear Hoechst staining as they travelled within the migration region using the TrackMate ImageJ plugin (*62*), and the total distance of each track was quantified.

Immunoprecipitation (IP) and western blotting

Cells were lysed in TGH (150 mM NaCl, 2 mM EGTA/EDTA, 50 mM HEPES (pH 7.4), 1% Triton X-100, 10% glycerol, 1 mM phenylmethylsulfonyl fluoride, 10 mM N-ethylmaleimide(NEM)) or RIPA (for immunoprecipitation; 50 mM Tris–HCl (pH 7.5), 150 mM NaCl, 1 mM EGTA, 1 mM EDTA, 1% Triton X-100, 1% Sodium deoxycholate, 0.2% SDS, 2.5 mM sodium pyrophosphate and 10 mM NEM), supplemented with Complete Mini EDTA-free protease inhibitor (Roche Applied Science, Heidelberg, Germany) and 100 µl phosphatase inhibitor cocktail 2 and 3 (P5726 and P0044, Sigma

586 Aldrich). Lysates were sonicated prior to centrifugation at 14 000 rpm for 10 min at 4°C
587 to separate non-soluble material. For immunoprecipitation, cell lysates were incubated
588 with 50 µl washed Protein G magnetic beads (10003D, Life Technologies) for 1 h at 4°C
589 to pre-clear the samples from unspecific binding proteins. Supernatants were incubated
590 with primary antibody alone for 2 h followed by the addition and overnight incubation
591 with Protein G magnetic beads at 4°C with agitation. SDS–PAGE was performed using the
592 X-cell II mini electrophoresis apparatus (Life Technologies) according to the
593 manufacturer's instructions. Samples were transferred to preactivated PVDF
594 membranes (Merck Millipore, Billerica, MA) and incubated with the respective primary
595 antibodies at 4°C overnight. Detection was performed using species-specific secondary
596 IR-Dye secondary antibodies (LI-COR Biosciences) and the Odyssey Infrared Imaging
597 System (LI-COR Biosciences). The integrated intensity of protein bands of interest was
598 measured using the ImageJ software and signals were normalised by dividing the
599 intensities of phosphorylated protein by total protein intensities or by dividing
600 intensities of co-immunoprecipitated proteins by the corresponding
601 immunoprecipitated protein.
602

603 **References:**

604

605 1. Y. Yarden, M. X. Sliwkowski, Untangling the ErbB signalling network. *Nature*
606 *Reviews Molecular Cell Biology* **2**, 127-137 (2001).

607 2. B. Snijder *et al.*, Population context determines cell-to-cell variability in endocytosis
608 and virus infection. *Nature* **461**, 520-523 (2009).

609 3. R. Kumar, H. Kuniyasu, C. D. Bucana, M. R. Wilson, I. J. Fidler, Spatial and temporal
610 expression of angiogenic molecules during tumor growth and progression. *Oncology*
611 *research* **10**, 301-311 (1998).

612 4. M. D. Ungrin, C. Joshi, A. Nica, C. Bauwens, P. W. Zandstra, Reproducible, Ultra
613 High-Throughput Formation of Multicellular Organization from Single Cell
614 Suspension-Derived Human Embryonic Stem Cell Aggregates. *PLoS ONE* **3**, (2008).

615 5. E. B. Pasquale, Eph receptors and ephrins in cancer: bidirectional signalling and
616 beyond. *Nature Reviews Cancer* **10**, 165-180 (2010).

617 6. H. Miao *et al.*, Activation of EphA receptor tyrosine kinase inhibits the Ras/MAPK
618 pathway. *Nature cell biology* **3**, (2001).

619 7. E. Batlle *et al.*, EphB receptor activity suppresses colorectal cancer progression.
620 *Nature* **435**, 1126-1130 (2005).

621 8. A. Merlos-Suárez, E. Batlle, Eph–ephrin signalling in adult tissues and cancer.
622 *Current Opinion in Cell Biology* **20**, 194-200 (2008).

623 9. C. Cortina *et al.*, EphB–ephrin-B interactions suppress colorectal cancer progression
624 by compartmentalizing tumor cells. *Nature Genetics* **39**, 1376-1383 (2007).

625 10. J. J. Li, D. P. Liu, G. T. Liu, D. Xie, EphrinA5 acts as a tumor suppressor in glioma by
626 negative regulation of epidermal growth factor receptor. *Oncogene* **28**, (2009).

627 11. A. W. Boyd, P. F. Bartlett, M. Lackmann, Therapeutic targeting of EPH receptors and
628 their ligands. *Nature Reviews Drug Discovery* **13**, 39-62 (2013).

629 12. H. Miao *et al.*, EphA2 mediates ligand-dependent inhibition and ligand-independent
630 promotion of cell migration and invasion via a reciprocal regulatory loop with Akt.
631 *Cancer cell* **16**, (2009).

632 13. J. W. Astin *et al.*, Competition amongst Eph receptors regulates contact inhibition of
633 locomotion and invasiveness in prostate cancer cells. *Nature Cell Biology* **12**, 1194-
634 1204 (2010).

635 14. G. Li *et al.*, EphB3 suppresses non-small-cell lung cancer metastasis via a
636 PP2A/RACK1/Akt signalling complex. *Nature communications* **3**, (2012).

637 15. B. Lin, T. Yin, Y. I. Wu, T. Inoue, A. Levchenko, Interplay between chemotaxis and
638 contact inhibition of locomotion determines exploratory cell migration. *Nature*
639 *Communications* **6**, 6619 (2015).

16. E. Er, M. C. Mendoza, A. M. Mackey, L. E. Rameh, J. Blenis, AKT facilitates EGFR trafficking and degradation by phosphorylating and activating PIKfyve. *Science signaling* **6**, (2013).

17. V. Laketa *et al.*, PIP_3 induces the recycling of receptor tyrosine kinases. *Science signaling* **7**, (2014).

18. G. Salazar, A. González, Novel mechanism for regulation of epidermal growth factor receptor endocytosis revealed by protein kinase A inhibition. *Molecular biology of the cell* **13**, 1677-1693 (2002).

19. S. S. Dykes, J. J. Steffan, J. A. Cardelli, Lysosome trafficking is necessary for EGF-driven invasion and is regulated by p38 MAPK and Na+/H+ exchangers. *BMC Cancer* **17**, 672 (2017).

20. H. Hanafusa *et al.*, Leucine-rich repeat kinase LRRK1 regulates endosomal trafficking of the EGF receptor. *Nature Communications* **2**, (2011).

21. J. Wang *et al.*, Activation of Rab8 guanine nucleotide exchange factor Rabin8 by ERK1/2 in response to EGF signaling. *Proceedings of the National Academy of Sciences* **112**, 148-153 (2015).

22. S. L. Schmid, Reciprocal regulation of signaling and endocytosis: Implications for the evolving cancer cell. *J Cell Biol* **216**, (2017).

23. S. Davis *et al.*, Ligands for EPH-related receptor tyrosine kinases that require membrane attachment or clustering for activity. *Science* **266**, 816-819 (1994).

24. O. Sabet *et al.*, Ubiquitination switches EphA2 vesicular traffic from a continuous safeguard to a finite signalling mode. *Nature Communications* **6**, 8047 (2015).

25. M. Baumdick *et al.*, EGF-dependent re-routing of vesicular recycling switches spontaneous phosphorylation suppression to EGFR signaling. *eLife* **4**, (2015).

26. S. Sigismund *et al.*, Threshold-controlled ubiquitination of the EGFR directs receptor fate. *The EMBO Journal* **32**, 2140-2157 (2013).

27. J. L. Macdonald, L. J. Pike, Heterogeneity in EGF-binding affinities arises from negative cooperativity in an aggregating system. *Proceedings of the National Academy of Sciences* **105**, 112-117 (2008).

28. D. Poteryaev, S. Datta, K. Ackema, M. Zerial, A. Spang, Identification of the Switch in Early-to-Late Endosome Transition. *Cell* **141**, 497-508 (2009).

29. J. W. Konturek, W. Bielanski, S. J. Konturek, J. Bogdal, J. Oleksy, Distribution and release of epidermal growth factor in man. *Gut* **30**, 1194-1200 (1989).

30. S. Sigismund *et al.*, Clathrin-Mediated Internalization Is Essential for Sustained EGFR Signaling but Dispensable for Degradation. *Developmental Cell* **15**, 209-219 (2008).

31. M. Offterdinger, V. Georget, A. Girod, P. I. H. Bastiaens, Imaging Phosphorylation Dynamics of the Epidermal Growth Factor Receptor. *Journal of Biological Chemistry* **279**, 36972-36981 (2004).

678 32. R. Villaseñor, Y. Kalaidzidis, M. Zerial, Signal processing by the endosomal system.
679 *Current Opinion in Cell Biology* **39**, 53-60 (2016).

680 33. A. Sorkin, M. von Zastrow, Endocytosis and signalling: intertwining molecular
681 networks. *Nature Reviews Molecular Cell Biology* **10**, 609-622 (2009).

682 34. N. Taub, D. Teis, H. L. Ebner, M. W. Hess, L. A. Huber, Late Endosomal Traffic of
683 the Epidermal Growth Factor Receptor Ensures Spatial and Temporal Fidelity of
684 Mitogen-activated Protein Kinase Signaling. *Molecular Biology of the Cell* **18**, 4698-
685 4710 (2007).

686 35. F. S. Wouters, P. Bastiaens, Fluorescence lifetime imaging of receptor tyrosine kinase
687 activity in cells. *Current Biology* **9**, 1127 (1999).

688 36. N. Verma *et al.*, PYK2 sustains endosomal-derived receptor signalling and enhances
689 epithelial-to-mesenchymal transition. *Nature Communications* **6**, 6064 (2015).

690 37. D. G. M. Guglielmo, P. C. Baass, W. J. Ou, B. I. Posner, J. J. Bergeron,
691 Compartmentalization of SHC, GRB2 and mSOS, and hyperphosphorylation of Raf-1
692 by EGF but not insulin in liver parenchyma. *The EMBO journal* **13**, 4269-4277
693 (1994).

694 38. D. Teis *et al.*, p14-MP1-MEK1 signaling regulates endosomal traffic and cellular
695 proliferation during tissue homeostasis. *The Journal of cell biology* **175**, 861-868
696 (2006).

697 39. S. Nada *et al.*, The novel lipid raft adaptor p18 controls endosome dynamics by
698 anchoring the MEK–ERK pathway to late endosomes. *The EMBO Journal* **28**, 477-
699 489 (2009).

700 40. A. Fortian, A. Sorkin, Live-cell fluorescence imaging reveals high stoichiometry of
701 Grb2 binding to the EGF receptor sustained during endocytosis. *Journal of Cell*
702 *Science* **127**, 432-444 (2014).

703 41. J. M. Haugh, T. Meyer, Active EGF receptors have limited access to PtdIns(4,5)P2 in
704 endosomes: implications for phospholipase C and PI 3-kinase signaling. *J. Cell Sci.*
705 **115**, (2002).

706 42. Y. Nishimura, S. Takiguchi, S. Ito, K. Itoh, EGF‐stimulated AKT activation is
707 mediated by EGFR recycling via an early endocytic pathway in a gefitinib‐resistant
708 human lung cancer cell line. *International journal of oncology* **46**, (2015).

709 43. R. Villaseñor, H. Nonaka, P. Conte-Zerial, Y. Kalaidzidis, M. Zerial, Regulation of
710 EGFR signal transduction by analogue-to-digital conversion in endosomes. *eLife* **4**,
711 (2015).

712 44. J. E. Ferrell, Jr, S. Ha, Ultrasensitivity part II: multisite phosphorylation,
713 stoichiometric inhibitors, and positive feedback. *Trends in Biochemical Sciences* **39**,
714 556-569 (2014).

715 45. M. Chinkers, J. A. McKanna, S. Cohen, Rapid induction of morphological changes in
716 human carcinoma cells A-431 by epidermal growth factors. *The Journal of Cell*
717 *Biology* **83**, 260-265 (1979).

718 46. A. J. Ridley, A. Hall, The small GTP-binding protein rho regulates the assembly of
719 focal adhesions and actin stress fibers in response to growth factors. *Cell* **70**, 389-399
720 (1992).

721 47. A. Y. Chan *et al.*, EGF stimulates an increase in actin nucleation and filament number
722 at the leading edge of the lamellipod in mammary adenocarcinoma cells. *Journal of*
723 *cell science* **111 (Pt 2)**, 199-211 (1998).

724 48. J. E. Segall *et al.*, EGF stimulates lamellipod extension in metastatic mammary
725 adenocarcinoma cells by an actin-dependent mechanism. *Clinical & Experimental*
726 *Metastasis* **14**, 61-72 (1996).

727 49. M. Bailly *et al.*, Relationship between Arp2/3 Complex and the Barbed Ends of Actin
728 Filaments at the Leading Edge of Carcinoma Cells after Epidermal Growth Factor
729 Stimulation. *The Journal of Cell Biology* **145**, 331-345 (1999).

730 50. B. D. Harms, G. M. Bassi, A. Horwitz, D. A. Lauffenburger, Directional Persistence
731 of EGF-Induced Cell Migration Is Associated with Stabilization of Lamellipodial
732 Protrusions. *Biophysical Journal* **88**, 1479-1488 (2005).

733 51. S.-C. Yip *et al.*, The distinct roles of Ras and Rac in PI 3-kinase-dependent protrusion
734 during EGF-stimulated cell migration. *Journal of Cell Science* **120**, 3138-3146 (2007).

735 52. M. El-Sibai *et al.*, Cdc42 is required for EGF-stimulated protrusion and motility in
736 MTLn3 carcinoma cells. *Journal of Cell Science* **120**, 3465-3474 (2007).

737 53. J. Li, M.-L. Lin, G. J. Wiepz, A. G. Guadarrama, P. J. Bertics, Integrin-mediated
738 Migration of Murine B82L Fibroblasts Is Dependent on the Expression of an Intact
739 Epidermal Growth Factor Receptor. *Journal of Biological Chemistry* **274**, 11209-
740 11219 (1999).

741 54. J.-M. Navenot, N. Fujii, S. C. Peiper, KiSS1 metastasis suppressor gene product
742 induces suppression of tyrosine kinase receptor signaling to Akt, tumor necrosis factor
743 family ligand expression, and apoptosis. *Molecular pharmacology* **75**, (2009).

744 55. J.-M. Navenot, N. Fujii, S. C. Peiper, Activation of Rho and Rho-Associated Kinase
745 by GPR54 and KiSS1 Metastasis Suppressor Gene Product Induces Changes of Cell
746 Morphology and Contributes to Apoptosis. *Molecular Pharmacology* **75**, 1300-1306
747 (2009).

748 56. A. Schenck *et al.*, The Endosomal Protein Appl1 Mediates Akt Substrate Specificity
749 and Cell Survival in Vertebrate Development. *Cell* **133**, 486-497 (2008).

750 57. M. Ebner, I. Lučić, T. A. Leonard, I. Yudushkin, PI(3,4,5)P3 Engagement Restricts
751 Akt Activity to Cellular Membranes. *Molecular Cell* **65**, 416-431000000 (2017).

752 58. M. Matsuda *et al.*, Real Time Fluorescence Imaging of Plcγ Translocation and Its
753 Interaction with the Epidermal Growth Factor Receptor. *The Journal of Cell Biology*
754 **153**, 599-612 (2001).

755 59. N. Jethwa *et al.*, Endomembrane PtdIns(3,4,5)P3 activates the PI3K–Akt pathway. *J*
756 *Cell Sci* **128**, 3456-3465 (2015).

60. T. L. Yuan, G. Wulf, L. Burga, L. C. Cantley, Cell-to-Cell Variability in PI3K Protein Level Regulates PI3K-AKT Pathway Activity in Cell Populations. *Current Biology* **21**, 173-183 (2011).

61. H. E. Grecco, P. Roda-Navarro, P. J. Verveer, Global analysis of time correlated single photon counting FRET-FLIM data. *Optics Express* **17**, 6493-6508 (2009).

62. J.-Y. Tinevez *et al.*, TrackMate: an open and extensible platform for single-particle tracking. *Methods*, (2016).

Acknowledgments: We would like to thank Dr. Astrid Krämer for critically reading this manuscript, Dr. Aneta Koseska for assistance in data analysis and Dr. Klaus Schuermann for generating the 3-D spatial-temporal maps. **Funding:** The project was partially funded by the European Research Council (ERC AdG 322637) to P.I.H.B. **Author contributions:** P.I.H.B. and W.S. conceived the project. W.S. performed and analyzed most experiments. O.S. performed experiments with LIFEA2 and contributed to the migration experiments, Y.B. contributed to the immunofluorescence experiments, L.B. contributed to the ICW and immunoprecipitation experiments. W.S. wrote the manuscript with assistance from P.I.H.B. **Competing interests:** The authors declare that no competing interests exist. **Data and material availability:** Data, scripts and reagents are available upon request.

779 **Figure Legends:**

780 **Figure 1: Eph receptor activation affects Akt-dependent EGFR trafficking. (A,B)**
781 Representative immunofluorescence images (A) and quantification (B) of endogenous
782 PM EGFR in Cos-7 cells (*N* = 16-29 cells/condition) following stimulation with ephrinA1-
783 Fc (A1, 2 μg/ml) for the indicated times (means ± sd). **(C)** Quantification of Akt
784 activation by In-cell Western (ICW) in Cos-7 cells following A1 stimulation (left: 2
785 μg/ml; right: 15 min) (means ± s.e.m.). **(D)** Quantification of endogenous PM EGFR
786 abundance by On-cell Western (OCW) and Akt activation in Cos-7 cells following
787 treatment with the Akt inhibitor AktVIII (10 μM) for the times indicated (means ±
788 s.e.m.). **(E)** EGF-Alexa647 binding (200 ng/ml, 2 min) to endogenous EGFR in Cos-7 cells
789 as a measure of PM EGFR abundance following 1 h pretreatment with A1 (2 μg/ml), the
790 PIKfyve inhibitor YM201636 (YM, 200 nM) or both (*N*=33-59 cells/condition) (means ±
791 sd). **(F)** Representative confocal images of Cos-7 cells expressing EGFR-mCherry before
792 (top left) and after (top right) treatment with AktVIII (10 μM, 1 h) and quantification of
793 the increase in endosomal EGFR-mCherry during AktVIII treatment (bottom, *N* = 6 cells,
794 means ± sd). **(G)** Representative time-lapse confocal images of Cos-7 cells expressing
795 EGFR-mCherry and EphA2-mCitrine following A1 stimulation (2 μg/ml). **(H)**
796 Quantification of endosomal EGFR-mCherry and EphA2-mCitrine from time-lapse
797 confocal imaging (G) during A1 stimulation (*N* = 7 cells, means ± sd). **(I)** Quantification
798 of PM EGFR-mCherry and EphA2-mCitrine abundance by OCW during A1 stimulation (2
799 μg/ml) (means ± s.e.m.). **(J)** Immunofluorescence measurements of EGFR intensity in
800 Rab5-, Rab5/Rab7- and Rab7-positive endosomal compartments in control, A1-(2
801 μg/ml, 1 h) and AktVIII-(10 μM, 1 h) pretreated Cos-7 cells prior to (left) and following
802 EGF stimulation (right, 100 ng/ml, 1 h). (*N*=6-11 cells/condition). Data are represented
803 by Tukey boxplots with the mean denoted as a cross and the median as a line. **(K)**

804 Measurements of EGFR recycling in control and A1-pretreated cells (2 μg/ml, 1 h) by
805 immunofluorescence prior to (pre), after EGF stimulation (10 ng/ml, 15 min) and 15
806 min following EGF washout (*N* = 34-40 cells/condition, means ± sd). Statistical
807 significance was determined in B, E, J and K using a one-way ANOVA with Sidak's *post-*
808 *hoc* test (***, $p < 0.001$). Scale bars = 20 μm.
809
810
811 **Figure 2: Eph receptor activation changes the spatial distribution of EGFR activity.**
812 **(A-B)** Average spatial-temporal maps (A) of endogenous EGFR abundance (top) and
813 Tyr^{845} phosphorylation (bottom) in radially segmented Cos-7 cells (plasma membrane,
814 PM → nuclear membrane, NM) prior to and during EGF stimulation (20 ng/ml for 5, 30
815 and 60 min) in control, ephrinA1-Fc- (A1, 2 μg/ml, 1 h), AktVIII- (10 μM, 1 h) and
816 YM201636- (YM, 200 nM, 1h) pretreated cells (*N* = 50-90 cells per condition). Single cell
817 measurements of EGFR $pTyr^{845}$ phosphorylation in the PM segment (B) during EGF
818 stimulation (means ± sd) **(C)** Phosphorylated fraction of EGFR-mCitrine as detected by
819 FLIM-FRET (α) and representative images of EGFR-mCitrine and EGF-Alexa647
820 fluorescence in control and A1- (2 μg/ml, 1 h), AktVIII- (10 μM, 1 h) and YM- (200 nM,
821 1h) pretreated Cos-7 cells following 60 min of EGF-Alexa647 stimulation (20 ng/ml) (*N*
822 = 10-14 cells/condition). **(D-F)** Quantification of the PM:endosome ratio of (D) EGFR-
823 mCitrine and (E) EGF-Alexa647 fluorescence intensity and **(F)** phosphorylated fraction
824 of EGFR-mCitrine (α) at PM and endosomes (means ± sd). Statistical significance was
825 determined in B and D-F using a one-way ANOVA with Sidak's *post-hoc* test (***, $p <$
826 0.001; **, $p < 0.01$; *, $p < 0.05$). Scale bars = 20 μm.
827
828

Figure 3: Eph receptor activation at cell-cell contact alters the EGFR signaling response. (A) Quantification of Akt (top) and ERK (bottom) activation by ICW in control and ephrinA1-Fc-pretreated (A1, 2 μg/ml, 1 h) Cos-7 cells endogenously expressing the receptors following EGF stimulation (1 ng/ml) (means ± s.e.m.) **(B)** Quantification of Akt activation in control or A1-pretreated (2 μg/ml, 1 h) HEK293 cells, followed by 30 min treatment with the dynamin inhibitor dynole 34-2 (100 μM, top) or its negative control analog dynole 31-2 (100 μM, bottom), then stimulated with EGF (1 ng/ml) for the times indicated (means ± s.e.m.) **(C)** Quantification of EGF-promoted Akt activation in Cos-7 cells following pretreatment with increasing concentrations of A1 (0.02, 0.2 and 2 μg/ml, 1 h) (means ± s.e.m.) **(D)** Representative images of EphA2 activity using a FRET-based sensor (LIFEA2(*24*)), whereby a decrease in fluorescence lifetime (τ, ns) represents an increase in activity, and fluorescence intensity measurements of LIFEA2-mCitrine and SH2-mCherry in Cos-7 cells. Scale bar = 20 μm. **(E,F)** Single cell measurements of Akt (E) and ERK (F) activation versus cell-cell contact in 2-D cultures (% cell circumference) in unstimulated and EGF stimulated (20 ng/ml, 1 h) Cos-7 cells. A sum-of-squares F test was used to determine significance: Akt, unstimulated: $F = 16.0$, $p = 0.001$, $r^2 = 0.432$; Akt, EGF: $F = 21.4$, $p < 0.001$, $r^2 = 0.322$; ERK, unstimulated: $F = 0.180$, $p = 0.673$, $r^2 = 0.003$; ERK, EGF: $F = 0.321$, $p = 0.575$, $r^2 = 0.009$.

Figure 4: Coupling EGFR activity to vesicular recycling generates a positive feedback. (A) Quantification of endogenous PM EGFR abundance and Akt activation in Cos-7 cells by OCW and ICW, respectively, following treatment with the PP2A inhibitor okadaic acid (OA, 1 μM, 2 h) (means ± s.e.m.) **(B)** Representative images and quantification of EGFR-paGFP recycling to the PM following endosomal photoactivation in Cos-7 cells (top) in control, EGF (20 ng/ml, 15 min), AktVIII (10 μM, 1 h) and AktVIII-

pretreated, EGF-stimulated (bottom, *N* = 6-10 cells/condition) (means ± s.e.m.) Scale bar = 20 μm **(C)** Spatial network topology showing positive feedback generated by coupling PM EGFR activity and Akt-dependent vesicular recycling. PIKfyve inhibition by YM201636 (YM) decouples Akt activation from its effect on EGFR recycling. **(D-E)** Single cell measurements of Akt phosphorylation by flow cytometry in control (top), YM- (200 nM, 1h, middle) and ephrinA1-Fc- (A1, 2 μg/ml, 1h, bottom) pretreated Cos-7 cells endogenously expressing the receptors following stimulation with EGF concentrations indicated (ng/ml, 1 h). (D) Solid lines represent the sum of two Gaussian fits for data accumulated from at least 10 000 cells per condition in 3-4 independent experiments. (E) Quantification of Akt activation for increasing concentrations of EGF. Circle sizes represent the relative proportions of the low (gray) and high (red) Akt activity populations estimated from the Gaussian distributions derived for each EGF concentration shown in D (means ± s.e.m.).

Figure 5: Eph activation at cell-cell contact suppresses the EGF-promoted transition to a migratory state. (A) Representative immunofluorescence images and **(B)** quantification of endogenous PM EGFR abundance in NIH 3T3 cells following ephrinA1-Fc (A1, 2 μg/ml) stimulation (means ± sd). Statistical significance was determined using a one-way ANOVA with Sidak's *post-hoc* test (***, $p < 0.001$; **, $p < 0.01$). **(C)** Percent of NIH 3T3 cells initiating a migratory response (top, means ± s.e.m) and the distance travelled by migratory cells (bottom, means ± s.d.) following EGF stimulation. Cells were pretreated with vehicle (control), YM201636 (YM, 200 nM, 1 h), or ephrinA1-Fc (A1, 2 μg/ml, 1h, green, or 0.02-2 μg/ml as indicated, red) followed by EGF stimulation (0-100 ng/ml as indicated) for 16 h. **(D)** Percent of migrating NIH 3T3 cells when seeded at low or high density in a single well following pretreatment with

vehicle or A1 (2 μg/ml, 1 h) and stimulated with EGF (20 ng/ml) for 16 h (means ± s.e.m). Data in C and D were obtained from least three independent experiments, consisting of at least two replicates per experiment (N = 581–1483 cells/condition) and statistical significance was determined using an ordinary one-way ANOVA with Holm-Sidak's multiple corrections *post-hoc* test. **(E)** Quantification of retinoblastoma (Rb) phosphorylation by ICW for vehicle- (control), A1- (2 μg/ml, 1 h) and YM- (200 nM, 1 h) pretreated NIH 3T3 cells following 24 h EGF stimulation at the concentrations indicated (means ± s.e.m).

Figure 6: Modulation of vesicular dynamics as a general mechanism to produce context-dependent EGFR signaling. (A) Quantification of Akt activation and PM EGFR abundance in HEK293 cells by ICW and OCW, respectively, following stimulation with kisspeptin-10 (Kp-10, 100 nM) (means ± s.e.m). **(B,C)** Quantification of Akt and ERK activation by ICW in HEK293 cells for control and Kp-10-pretreated (100 nM, 1 h) cells following EGF stimulation (1 ng/ml) (means ± s.e.m).

Supplementary Materials

Figure S1: Eph receptor activation reduces PM EGFR abundance.

Figure S2: Akt/PIKfyve regulates EGFR vesicular trafficking.

Figure S3. Akt is preferentially activated at the PM following EGFR stimulation.

Figure S4. EphrinA1-Fc pretreatment inhibits EGFR-promoted Akt activation.

Figure S5: Distributions of cell migration distances.

Movie S1: Akt inhibition induces EGFR endosomal accumulation.

Movie S2: EphrinA1-Fc stimulation induces EGFR endosomal accumulation.

Movie S3: EphrinA1-Fc:EphA2 interactions at cell-cell contact induces EGFR endosomal accumulation.

Movie S4: EGF-promoted migration in NIH 3T3 cells.

Supplementary Material Legends:

Figure S1: Eph receptor activation reduces PM EGFR abundance. (A-D) Quantification of endogenous PM EGFR abundance by ICW following ephrinA1-Fc stimulation (A1, 2 μg/ml) of (A) HEK293, (B) NIH 3T3, (C) MCF10A and (D) MDA-MB-231 cells. (means ± s.e.m) (E) Single cell immunofluorescence measurements of EGFR expression in the cell lines used in this study. (F-G) Cos-7 lysates immunoprecipitated (IP) with anti-EGFR (left) or blotted for total proteins (right) following stimulation with EGF (100 ng/ml) or A1 (2 μg/ml) for the indicated times. IP was probed with anti-HA (to detect co-transfected HA-ubiquitin), anti-pTyr^{845}, anti-pTyr^{1068}, anti-pTyr^{1045} (to detect phosphorylated EGFR) and anti-EGFR. Total lysates were probed with anti phospho-Eph (pEph), anti-EphA2, anti-pTyr^{1068}, anti-EGFR and anti-tubulin. Shown are (F) representative blots and (G) quantification of EGFR phosphorylation (pTyr^{845}) from four

921 independent experiments (means ± s.e.m). Statistical significance was determined using
922 a one-way ANOVA with Sidak's *post-hoc* test (**, $p < 0.01$).
923
924 **Figure S2: Akt/PIKfyve regulates EGFR vesicular trafficking.** (A) Representative
925 images and (B) quantification of endosomal EGFR-mCherry following treatment with the
926 PIKfyve inhibitor YM201636 (YM, 200 nM, 1h) ($N = 9$, mean ± s.e.m). Statistical
927 significance was determined using a two-tailed Student's t test. Scale bar = 20 μm. (C)
928 ICW measurements of total EGFR abundance following EGF stimulation (1-200 ng/ml,
929 30 min) in vehicle (control) and AktVIII (10 μM, 1 h) pretreated cells (means ± s.e.m).
930 Statistical significance was determined using a two-way ANOVA with Sidak's multiple
931 corrections *post-hoc* test (***, $p > 0.001$; **, $p > 0.01$).
932
933 **Figure S3. Akt is preferentially activated at the PM following EGFR stimulation.** (A)
934 Akt rapidly translocates to regions of EGF-bound receptors at the PM, but is not
935 recruited to endosomes following internalization of ligand-bound receptor. Shown are
936 representative images of Cos-7 cells expressing EGFR-mCitrine and PH-Akt-Cerulean
937 following stimulation with EGF-Alexa647 (100 ng/ml) for the indicated times. (B)
938 Colocalization between EGF-Alexa647 and PH-Akt-Cerulean is highest immediately after
939 stimulation (2 min) while most EGFR-mCitrine is localized at the plasma membrane. As
940 EGF-Alexa647 accumulates in endosomes (20 and 40 min), colocalization with PH-Akt-
941 Cerulean decreased. Quantification of colocalization by Mander's coefficient from EGF-
942 Alexa647 intensity-dependent thresholded images (means ± sd, $N = 4$). (C) Inhibition of
943 endocytosis increases EGF-promoted Akt activation, while ERK activation is decreased.
944 PM EGFR abundance was quantified by OCW and Akt/ERK activation by ICW in HEK293
945 cells stimulated with EGF (1 ng/ml) for the indicated times following pretreatment with

946 the dynamin inhibitor dynole 34-2 (100 μM, 30 min) or its negative control analog
947 dynole 31-2 (100 μM, 30 min) (means ± s.e.m). (D) Akt activation is rapidly terminated
948 following EGF washout in Cos-7 cells, indicating the necessity of PM EGF binding for
949 persistent Akt activation. ERK activation decays much slower following EGF removal
950 through due to persistent activity of endosomal EGFR. Akt and ERK activation were
951 measured by ICW following sustained EGF (1 ng/ml) stimulation or a 5 min EGF pulse
952 and subsequent washout (means ± s.e.m). Statistical significance was determined in B
953 using a repeated measures one-way ANOVA with a Dunnett's *post-hoc* test, and in C
954 using a two-way ANOVA with Sidak's *post-hoc* test. (***, $p < 0.001$; **, $p < 0.01$; *, $p <$
955 0.05). Scale bars = 20 μm

956
957

958 **Figure S4. EphrinA1-Fc pretreatment inhibits EGFR-promoted Akt activation.** Akt
959 and ERK activation were quantified by ICW in (A) Cos-7 cells ectopically expressing
960 EGFR and EphA2, and in (B) HEK293 cells endogenously expressing the receptors. Cells
961 were pretreated with vehicle (control) or ephrinA1-Fc (A1, 2 μg/ml) for 1 h, followed by
962 1 ng/ml EGF stimulation for the indicated times. Data represent means ± s.e.m.

963

964 **Figure S5: Distributions of cell migration distances.** Migration distance was
965 quantified for individual cells as described in *Methods*. Shown are the distributions of
966 migration distance for (A) all tracked cells (N = 32 203 cells) and (B) 20 ng/ml EGF
967 treated cells (N = 2343 cells). To distinguish migrating cells from those that are pushed
968 into the cell-free area by population expansion due to cell division during the 16 h
969 acquisition time, a minimal displacement distance of 0.01 cm was used as a threshold.

970

971 **Movie S1: Akt inhibition induces EGFR endosomal accumulation.** Treatment of Cos-
972 7 cells ectotopically expressing EGFR-mCherry with the Akt inhibitor AktVIII (10 μM)
973 promotes an increase in endosomal EGFR. Scale bar = 20 μm
974
975 **Movie S2: EphrinA1-Fc stimulation induces EGFR endosomal accumulation.**
976 Stimulation of Cos-7 cells ectotopically expressing EGFR-mCherry and EphA2-mCitrine
977 with EphrinA1-Fc (2 μg/ml) promotes an increase in endosomal EGFR. Scale bar = 20
978 μm
979
980 **Movie S3: EphrinA1-Fc:EphA2 interactions at cell-cell contact induces EGFR**
981 **endosomal accumulation.** HEK293 cells ectopically expressing EBFP-EphrinA1 in
982 suspension were added to adherent Cos-7 cells ectopically expressing EGFR-mCherry
983 and EphA2-mCitrine 30 min prior to imaging. Time lapse imaging begins as EBFP-
984 EphrinA1-HEK293T cells make initial cell-cell contact with Cos-7 cells. Scale bar = 20 μm
985
986 **Movie S4: EGF-promoted migration in NIH 3T3 cells.** Unstimulated (unstim), EGF (20
987 ng/ml), YM201636 (200 nM) followed by EGF (20 ng/ml) stimulation (YM) and
988 EphrinA1-Fc (2 μg/ml) followed by EGF (20 ng/ml) stimulation (A1). Scale bar = 100
989 μm
990

Figure 1

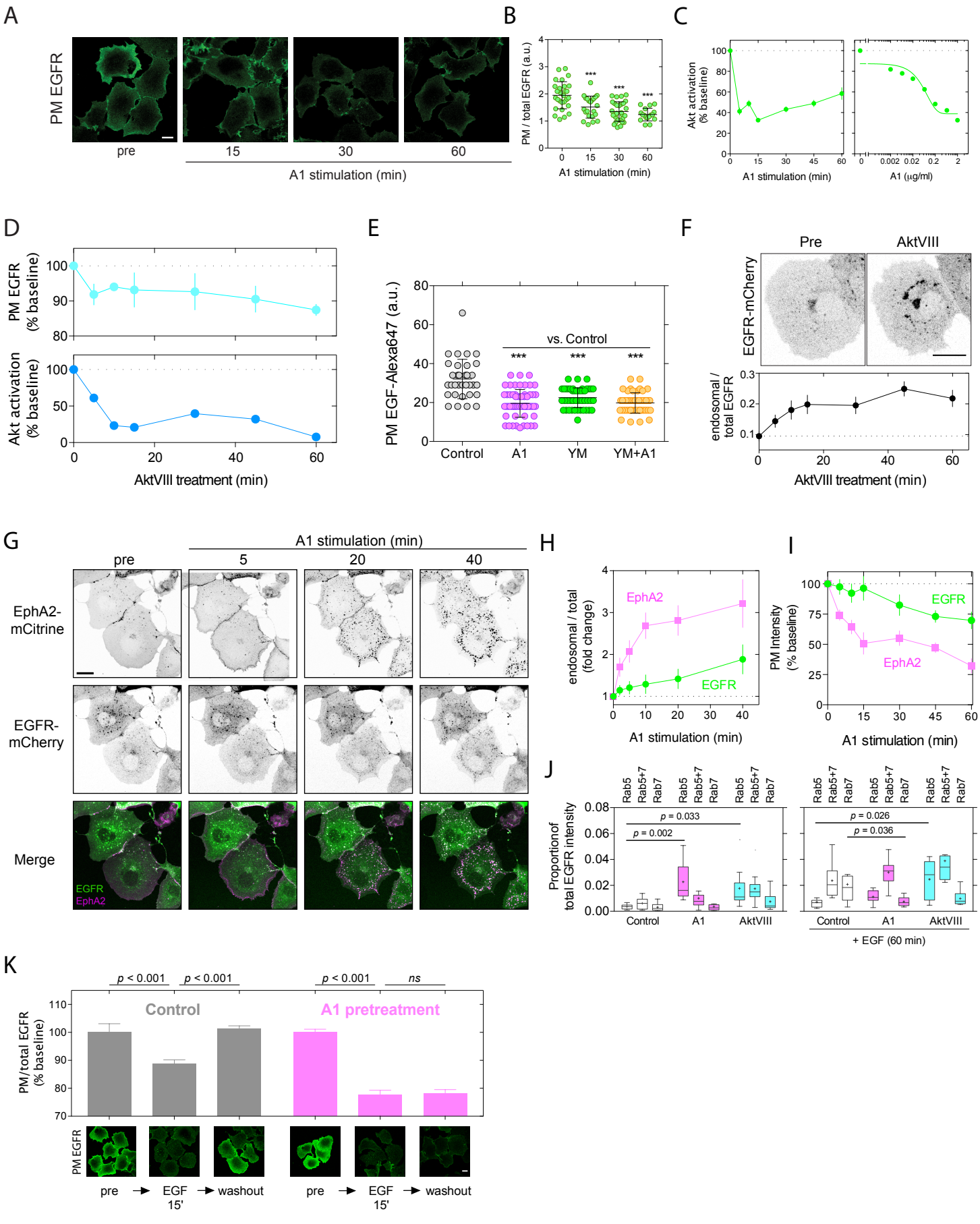
A
PM EGFR
pre
15
30
60
A1 stimulation (min)
B
PM / total EGFR (a.u.)
A1 stimulation (min)
C
Akt activation (% baseline)
A1 stimulation (min)
A1 (μg/ml)
D
PM EGFR (% baseline)
Akt activation (% baseline)
AktVIII treatment (min)
E
PM EGF-Alexa647 (a.u.)
vs. Control
Control
A1
YM
YM+A1
F
Pre
AktVIII
EGFR-mCherry
endosomal / total EGFR
AktVIII treatment (min)
G
A1 stimulation (min)
pre
5
20
40
EphA2-mCitrine
EGFR-mCherry
Merge
EGFR
EphA2
H
endosomal / total (fold change)
EphA2
EGFR
A1 stimulation (min)
I
PM Intensity (% baseline)
EGFR
EphA2
A1 stimulation (min)
J
Proportionof total EGFR intensity
Rab5
Rab5+7
Rab7
p = 0.033
p = 0.002
p = 0.026
p = 0.036
Control
A1
AktVIII
+ EGF (60 min)
K
p < 0.001
p < 0.001
p < 0.001
ns
Control
A1 pretreatment
PM/total EGFR (% baseline)
PM EGFR
pre
EGF 15'
washout

Figure 2

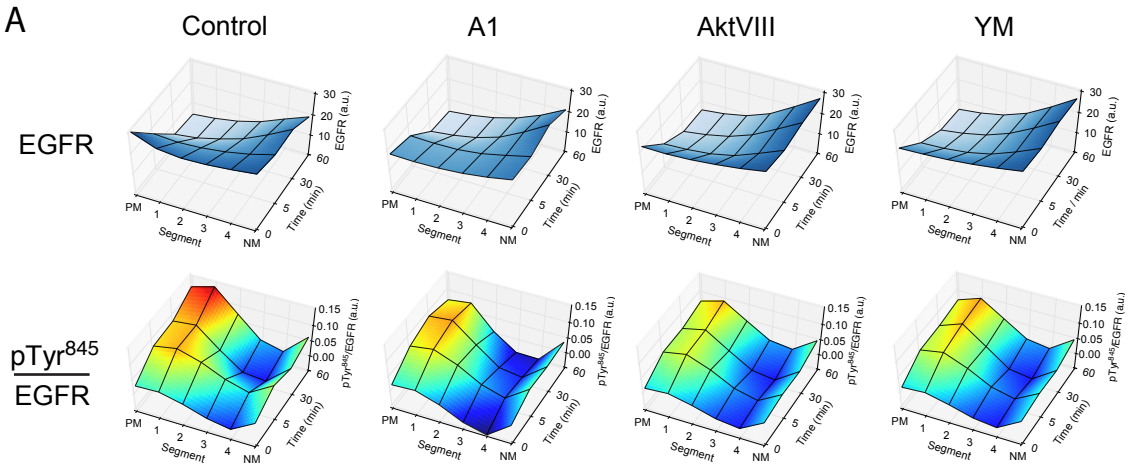
A
Control
A1
AktVIII
YM
EGFR
pTyr845/EGFR
EGFR (a.u.)
pTyr845/EGFR (a.u.)
Segment
Time (min)
PM
NM

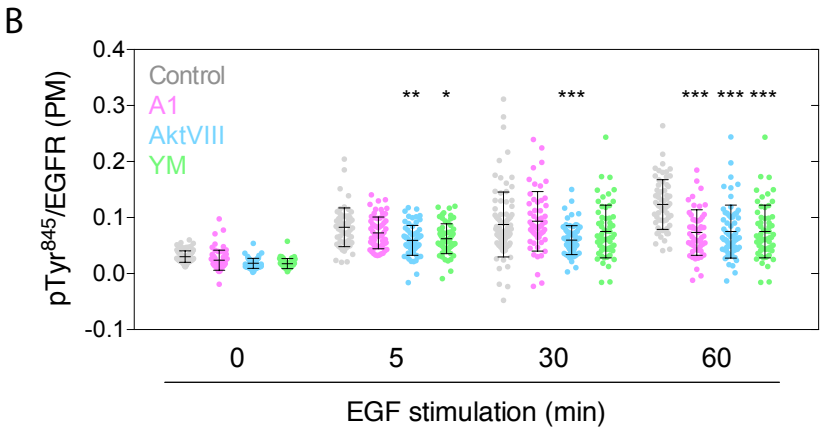
B
Control
A1
AktVIII
YM
pTyr845/EGFR (PM)
EGF stimulation (min)

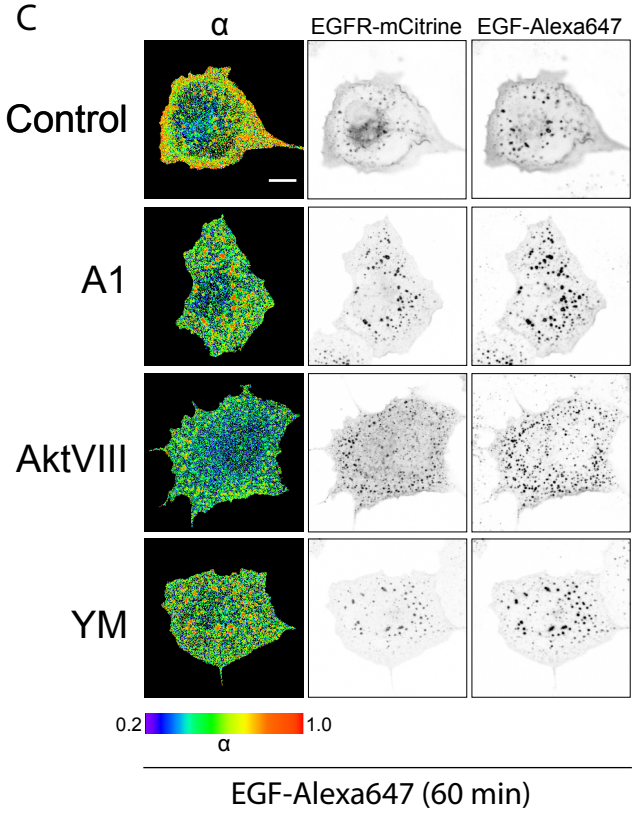
C
α
EGFR-mCitrine
EGF-Alexa647
Control
A1
AktVIII
YM
EGF-Alexa647 (60 min)

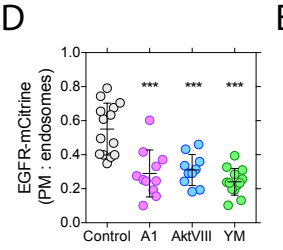
D
EGFR-mCitrine (PM : endosomes)
Control
A1
AktVIII
YM

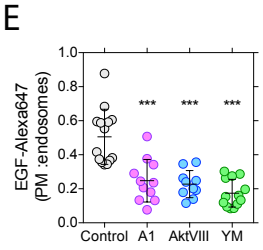
E
EGF-Alexa647 (PM :endosomes)
Control
A1
AktVIII
YM

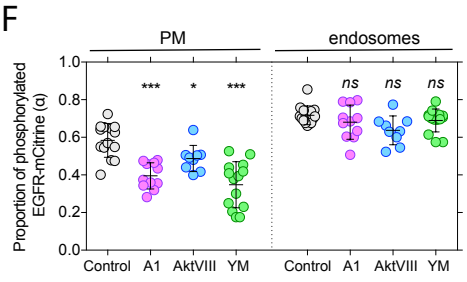
F
PM
endosomes
Proportion of phosphorylated EGFR-mCitrine (α)
Control
A1
AktVIII
YM

Figure 3

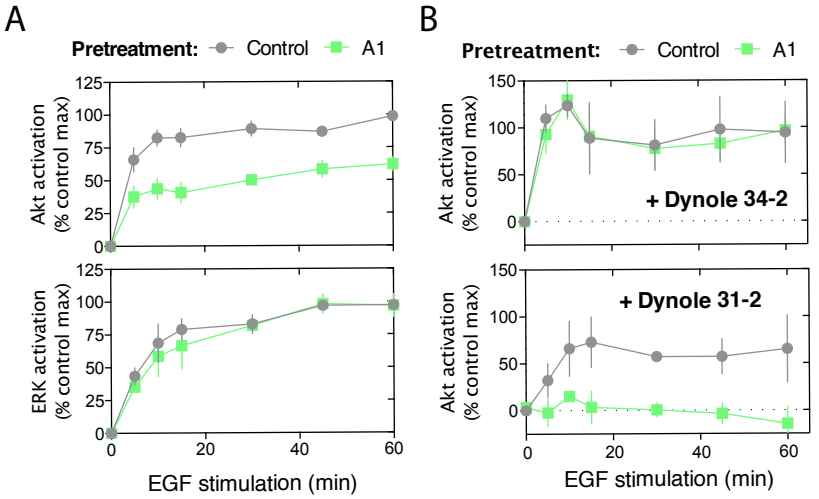
A
Pretreatment: Control A1
Akt activation (% control max)
ERK activation (% control max)
EGF stimulation (min)
B
Pretreatment: Control A1
+ Dynole 34-2
+ Dynole 31-2
Akt activation (% control max)
EGF stimulation (min)

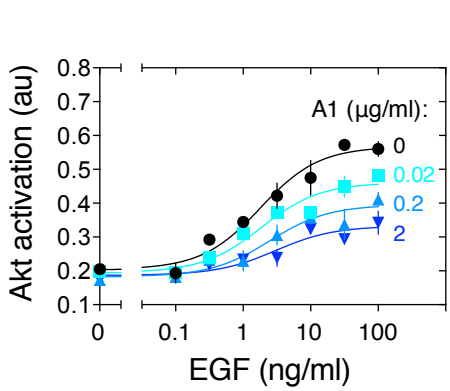
C
Akt activation (au)
A1 (µg/ml):
0
0.02
0.2
2
EGF (ng/ml)

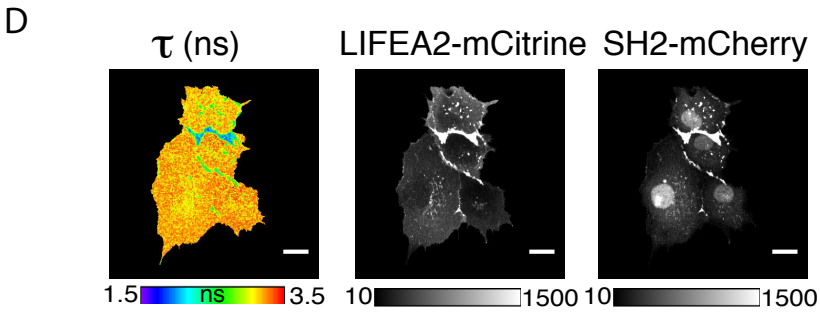
D
τ (ns)
LIFEA2-mCitrine
SH2-mCherry
1.5
ns
3.5
10
1500
10
1500

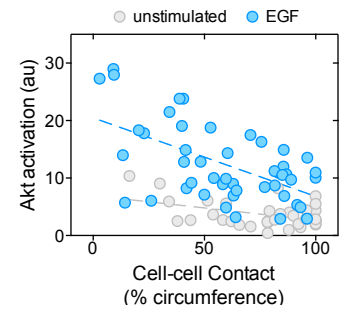
E
unstimulated
EGF
Akt activation (au)
Cell-cell Contact
(% circumference)

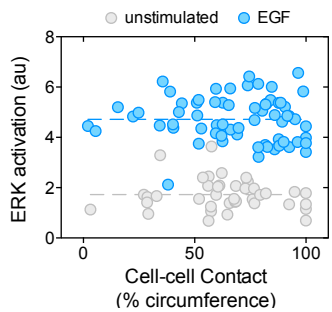
F
unstimulated
EGF
ERK activation (au)
Cell-cell Contact
(% circumference)

Figure 4

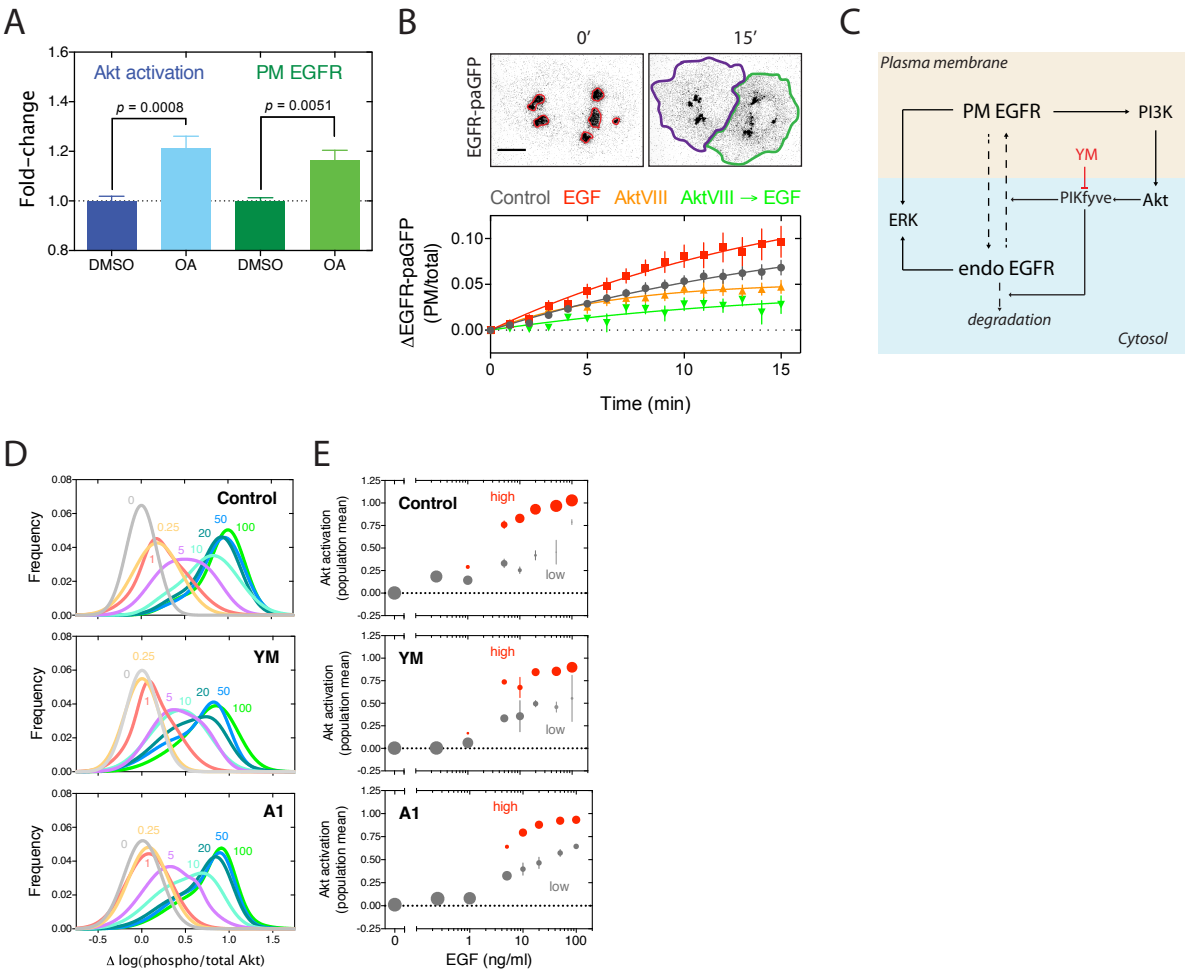
A
Akt activation
PM EGFR
p = 0.0008
p = 0.0051
Fold-change
DMSO
OA
DMSO
OA
B
0′
15′
EGFR-paGFP
Control
EGF
AktVIII
AktVIII → EGF
ΔEGFR-paGFP (PM/total)
Time (min)
C
Plasma membrane
PM EGFR
PI3K
YM
PIKfyve
Akt
ERK
endo EGFR
degradation
Cytosol

D
Control
YM
A1
Frequency
Δ log(phospho/total Akt)
E
Control
YM
A1
high
low
Akt activation (population mean)
EGF (ng/ml)

Figure 5

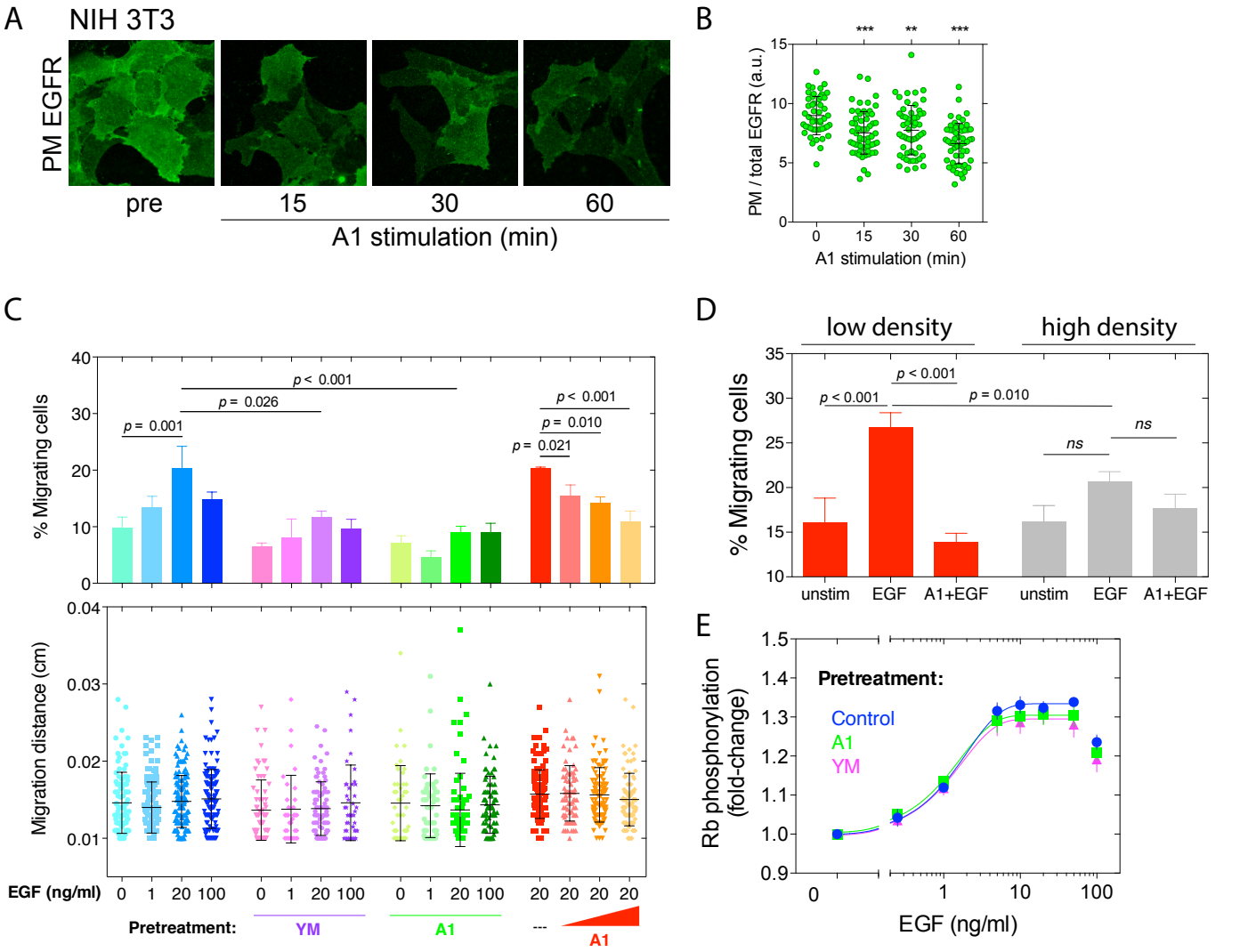

Figure 6

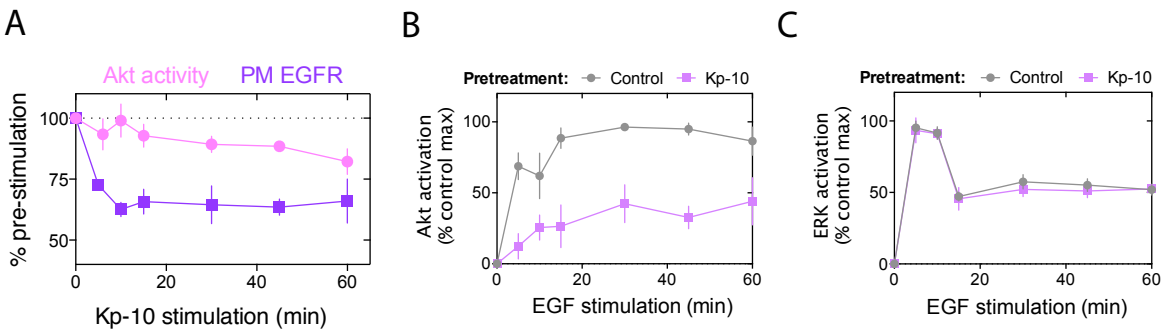
A
Akt activity
PM EGFR
% pre-stimulation
100
75
50
0
20
40
60
Kp-10 stimulation (min)
B
Pretreatment:
Control
Kp-10
Akt activation
(% control max)
100
50
0
0
20
40
60
EGF stimulation (min)
C
Pretreatment:
Control
Kp-10
ERK activation
(% control max)
100
50
0
0
20
40
60
EGF stimulation (min)

Figure S1

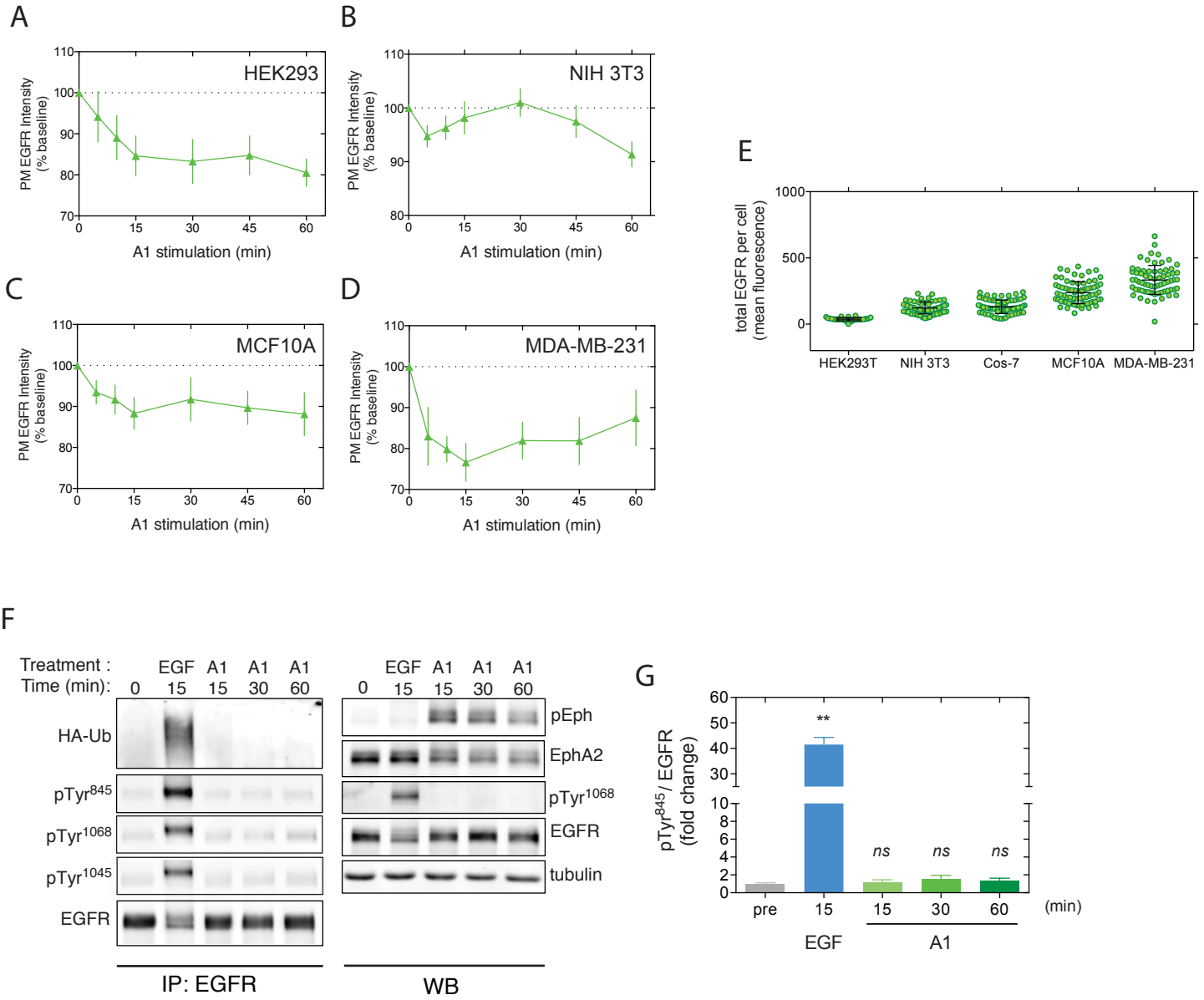

Figure S2

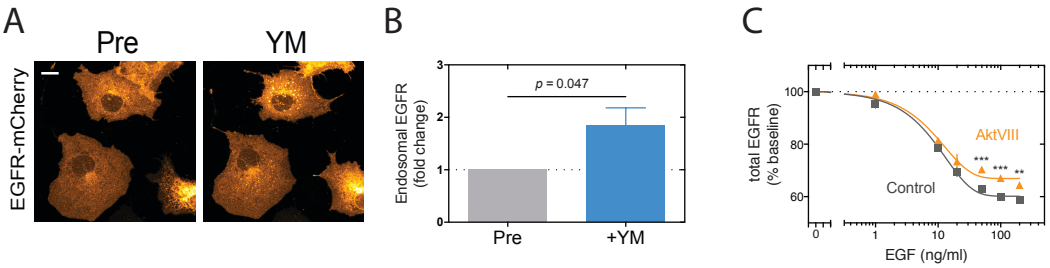

Figure S3

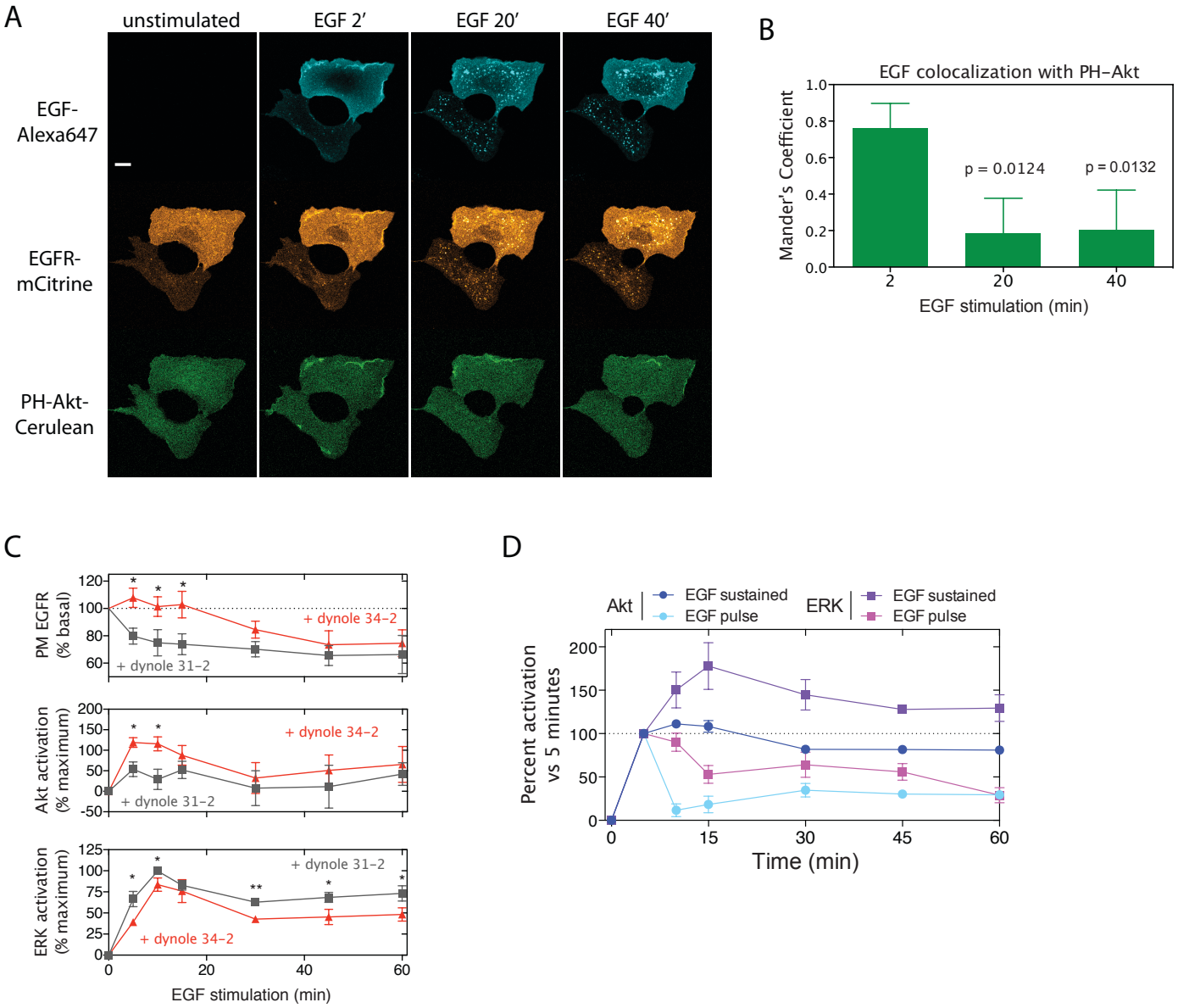

Figure S4

A

Cos-7 (+EGFR/EphA2)

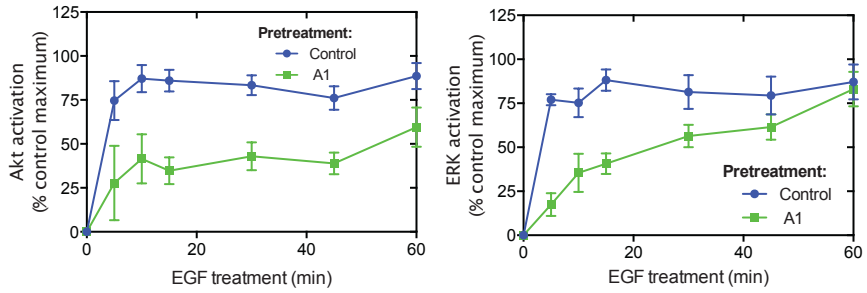

B

HEK293

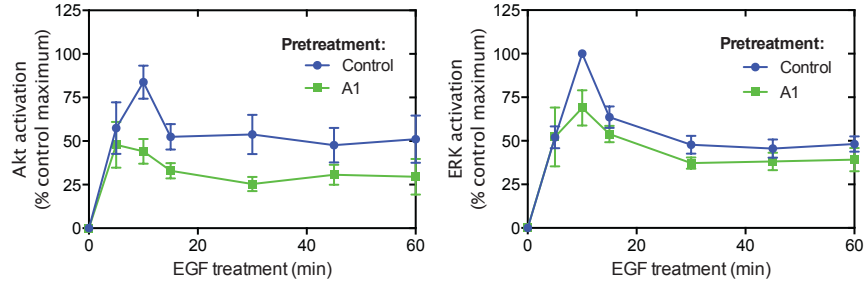

Figure S5

A

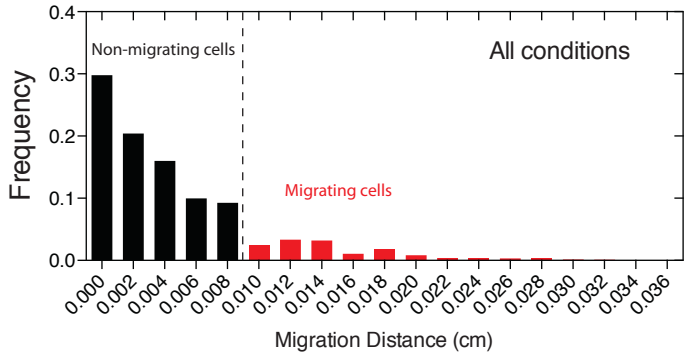

B